Cardiac Output Estimation using Arterial Blood Pressure Waveforms

by

James Xin Sun

Bachelor of Science in Electrical Engineering and Computer Science (Massachusetts Institute of Technology, 2005)

Submitted to the Department of Electrical Engineering and Computer Science
in partial fulfillment of the requirements for the degree of

Master of Engineering in Electrical Engineering and Computer Science

at the

MASSACHUSETTS INSTITUTE OF TECHNOLOGY

September 2006

Author .....
Department of Electrical Engineering and Computer Science
September 1, 2006

Certified by .....
Roger G. Mark
Distinguished Professor in Health Sciences and Technology
Professor of Electrical Engineering
Thesis Supervisor

Accepted by .....
Arthur C. Smith
Chairman, Department Committee on Graduate Students

Cardiac Output Estimation using Arterial Blood Pressure Waveforms

by

James Xin Sun

Submitted to the Department of Electrical Engineering and Computer Science
on September 1, 2006, in partial fulfillment of the
requirements for the degree of
Master of Engineering in Electrical Engineering and Computer Science

Abstract

Cardiac output (CO) is a cardinal parameter of cardiovascular state, and a fundamental determinant of global oxygen delivery. Historically, measurement of CO has been limited to critically-ill patients, using invasive indicator-dilution methods such as thermodilution via Swan-Ganz lines, which carry risks. Over the past century, the premise that CO could be estimated by analysis of the arterial blood pressure (ABP) waveform has captured the attention of many investigators. This approach of estimating CO is minimally invasive, cheap, and can be done continuously as long as ABP waveforms are available. Over a dozen different methods of estimating CO from ABP waveforms have been proposed and some are commercialized. However, the effectiveness of this approach is nebular. Performance validation studies in the past have mostly been conducted on a small set of subjects under well-controlled laboratory conditions. It is entirely possible that there will be circumstances in real world clinical practice in which CO estimation produces inaccurate results.

In this thesis, our goals are to (1) build a computational system that estimates CO using 11 of the established methods; (2) evaluate and compare the performance of the CO estimation methods on a large set clinical data, using the simultaneously available thermodilution CO measurements as gold-standard; and (3) design and evaluate an algorithm that identifies and eliminates ABP waveform segments of poor quality.

Out of the 11 CO estimation methods studied, there is one method (Liljestrand method) that is clearly more accurate than the rest. Across our study population of 120 subjects, the Liljestrand method has an error distribution with a 1 standard deviation error of 0.8 L/min, which is roughly twice that of thermodilution CO. These results suggest that although CO estimation methods may not generate the most precise values, they are still useful for detecting significant (>1 L/min) changes in CO.

Thesis Supervisor: Roger G. Mark
Title: Distinguished Professor in Health Sciences and Technology
Professor of Electrical Engineering

Acknowledgments

This research would not have been possible without the help and support of many people.

First, I thank my thesis supervisor, Prof. Roger G. Mark. Your advice, support, care, and friendship are the reasons for the success of this thesis. Your leadership is truly inspiring. You have opened my eyes to the vast field of biomedical engineering, and I fully intend to pursue this field for the rest of my life.

I owe a great deal to Dr. Andrew Reisner and Mohammed Saeed. They introduced me to the area of cardiac output estimation. Their help and support unquestionably shaped the scope of my research.

I thank all members of the Lab for Computational Physiology and members of the BRP. It is because of them I enjoyed being at the lab almost every day. Thanks to Dr. Gari Clifford for all the signal processing advice and his British sense of humor; to Dr. Thomas Heldt for his technical advice and of course, for his self-confident attitude; to Tushar Parlikar for keeping this final semester so entertaining; to Mauricio Villarroel, the UNIX guru, for the database and Linux support; to Anton Aboukhalil for his magic tricks.

I thank all my friends at MIT. Dearest thanks to every member of the "little-family" for all those get-togethers and birthday showerings: I will treasure all those memorable moments; to Tin, the "free electricity" Burmese, for being a great friend and lab-mate at LCP.

I sincerely thank my family (mom, dad, Andrew) for all their encouragement, love, and support.

This work was made possible by grant R01 EB001659 from the National Institute of Biomedical Imaging and Bioengineering.

Contents

List of Figures

List of Tables

Chapter 1

Introduction

1.1 Motivation

The cardiovascular system provides vital nutrients and removes wastes from body tissues. The powerhouse of the cardiovascular system is the heart, pumping out oxygenated blood to the systemic circulation (Figure 1-1). For a normal healthy adult at rest, cardiac output (CO), the average flow rate of blood pumped into the aorta, is approximately 5 liters per minute. For an Olympic athlete at maximum workout, CO exceeds 30 L/min. For a patient in circulatory shock, CO can be less than 2 L/min. The tremendous dynamic range suggests that CO is a key indicator of one's hemodynamic state. Thus, it would be a tremendous asset to determine CO accurately, reliably, and continuously using minimally invasive methods.

1.1.1 Measurement of cardiac output

Flowmeter. The most direct and accurate way of measuring CO is to use a flowmeter. One could conceivably place an ultrasonic flow probe around a major vessel protruding from the heart such as the aorta. Instantaneous pulsatile flow is obtained with a millisecond time resolution. Stroke volume, the volume of blood ejected into the aorta per cardiac cycle, is calculated by integrating the flow curve over a cardiac cycle. CO is then obtained by multiplying stroke volume with heart rate. Unfortunately, this direct flow measurement requires thoracotomy (surgical incision of the chest wall), which is impractical to perform in humans just for diagnostic purposes.

Fick principle. A more practical way to obtain CO is through the Fick principle of O_2 mass balance. It states that the amount of O_2 consumed must equal the difference in O_2 quantity between the arterial and venous circulation. Using this fact, CO is obtained as follows:

$$\mathrm{CO} = \frac{\mathrm{O_2\ consumption}}{\mathrm{arterial\ O_2\ content - mixed\ venous\ O_2\ content}} \quad \frac{[\mathrm{L\ O_2/min}]}{[\mathrm{L\ O_2/L\ blood}]}$$

Therefore, to determine CO, O_2 consumption and content in blood need to be measured.

Thermodilution. Another clinically plausible method of obtaining CO is through an indicator dilution technique, which is based upon conservation of the indicator solution. As shown in Figure 1-2, cardiac output Q flows entirely through a large vessel. A known amount of dye is injected at point A, and concentration as a function of time is measured

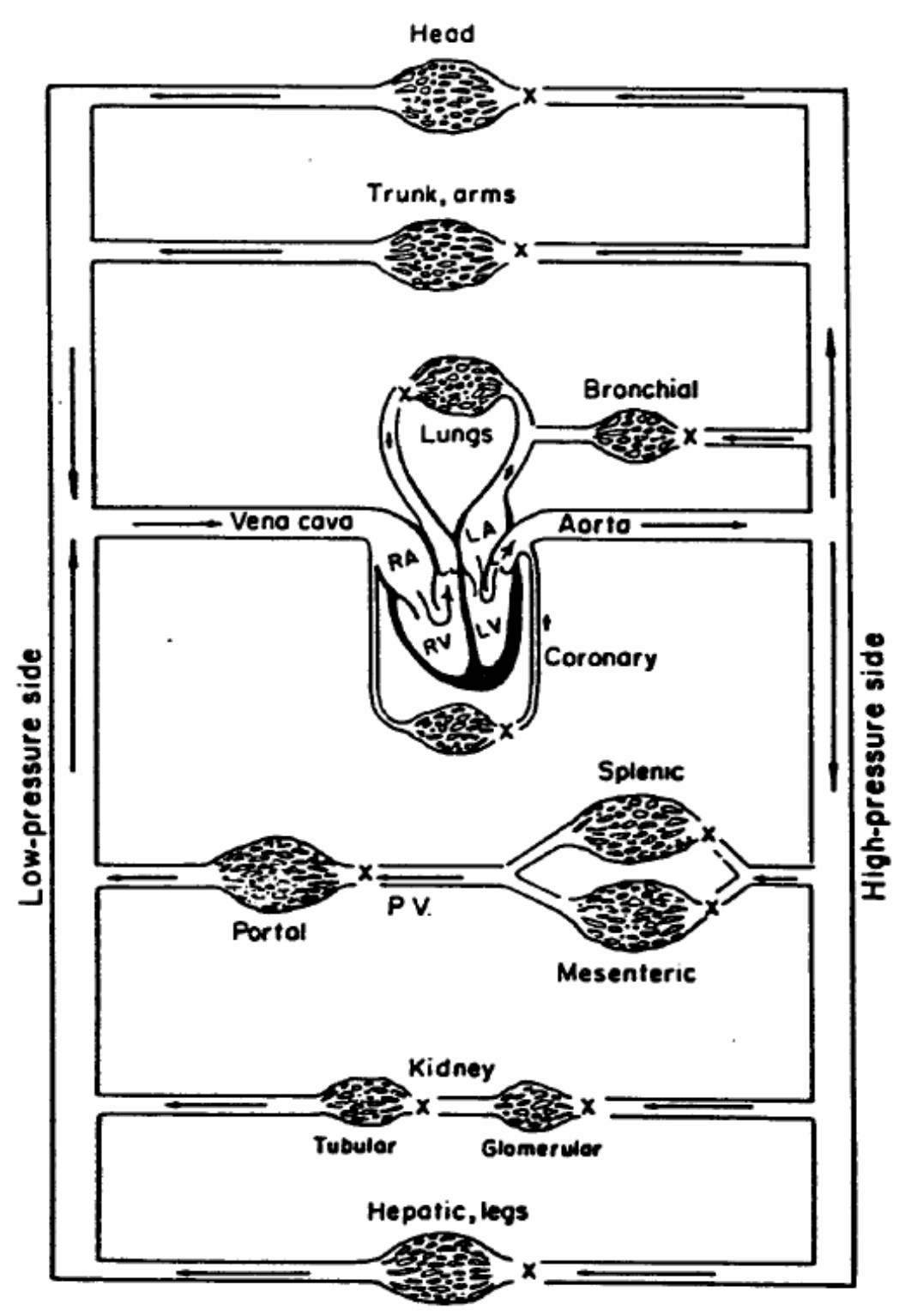

Figure 1-1: The cardiovascular system. Figure adapted from [13].

downstream at point B. By dye conservation, the amount injected must pass through point B, and CO is obtained as follows:

$$\text{CO} = \frac{q}{\int_{t_1}^{t_2} c(t)dt} \quad \frac{[\text{mg}]}{[\text{mg·min/(L blood)}]}$$

Clinically, the most popular indicator dilution technique is thermodilution, in which cold saline of precisely known volume and temperature is injected, and then the temperature profile is measured downstream.

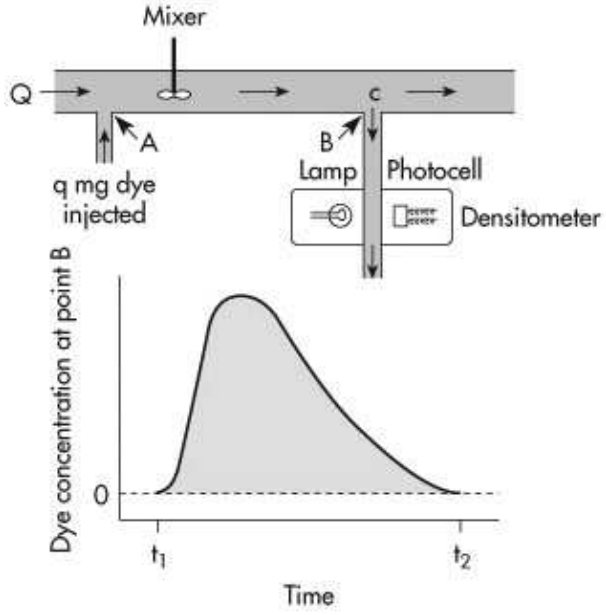

Figure 1-2: Indicator dilution principle. Figure adapted from [2].

Doppler ultrasound. More recently, a completely noninvasive method known as doppler ultrasound has been developed to measure CO [8]. This technique measures the aorta's instantaneous blood flow velocity $v(t)$ and cross sectional area A. Then stroke volume can be calculated by integrating $v(t)$ over a cardiac cycle of duration T:

$$SV = A \int_T v(t)dt$$

Remarks. Although the Fick method and thermodilution are both clinically feasible, they are still quite invasive and can only be performed in well-equipped environments like intensive care units (ICUs) and cardiac catheterization labs. Measurement of mixed venous O_2 requires a blood sample from the pulmonary artery. Injection of cold saline must be into a major vessel through which the entire CO flows. Consequently, a Swan-Ganz catheter that is threaded through the vena cava, through the right heart, and into the pulmonary artery is used to facilitate thermodilution CO measurements. Doppler ultrasound, while completely noninvasive and reasonably accurate, is expensive. Running this device requires costly equipment and an expert technician. In addition, none of the methods discussed in this section are practical for continuous bedside monitoring of a patient's CO.

1.1.2 Estimating cardiac output from arterial blood pressure

Throughout the past century, the premise that CO could be estimated by analysis of the arterial blood pressure (ABP) waveform (Figure 1-3) has captured the attention of many investigators. More than a dozen methods of calculating CO from ABP have been proposed, many of which are now commercially available. This approach to determine CO has the following advantages:

- Obtaining ABP is non-invasive or minimally invasive.
- ABP waveforms are routinely measured in clinical settings such as ICUs.
- The ABP waveform is measured continuously, allowing for continuous CO estimates.
- Cost benefits: The transformation from ABP to CO requires only numerical computation. No expensive equipment or expert technicians are required.

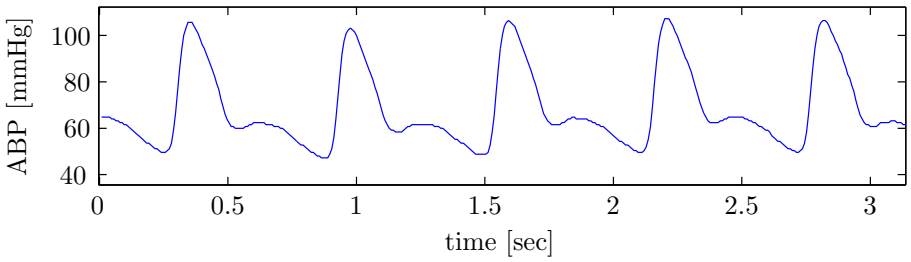

Figure 1-3: The arterial blood pressure (ABP) waveform.

To understand the relation between pressure (ABP) and flow (CO), we first start with a very simple representation of the cardiovascular system. Shown in Figure 1-4, there are two blocks: the heart and the systemic circulation. Blood flows out of the heart with a rate of $q(t)$ and a corresponding arterial pressure $P(t)$. Assuming that the internal state of the heart and the systemic circulation does not change, then it is plausible that higher flow corresponds to higher pressure. Unfortunately, in real life, system states such as systemic resistance can dynamically change within seconds, giving rise to a much more complicated pressure-flow relationship. The dozen or so methods of determining flow from pressure use cardiovascular system models and represent the internal structure of the two blocks in Figure 1-4 with varying levels of complexity, thereby quantitatively relating $P(t)$ and $q(t)$.

Having so many different $P - q$ relations existing today suggests that there is no consensus as to which method works best. Studies conducted in the past have mostly been on animals or a small set of human subjects under well-controlled laboratory conditions. The CO estimators have not been extensively evaluated with a large set of clinical ABP waveforms, hence the performance of CO estimation is still uncertain. It is entirely possible that there will be circumstances in real world clinical practice in which these indirect methods produce unacceptable estimates. The main goal of the research presented in this thesis is to determine the performance of the CO estimators.

1.1.3 MIMIC II database & data quality

Before evaluating the performance of CO estimation, we must first establish a suitable study population that contains ABP waveform data and contemporaneous reference CO

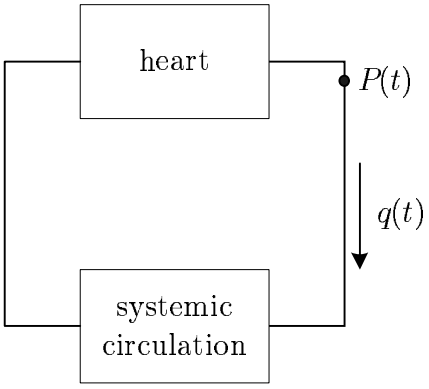

Figure 1-4: A simple, lumped cardiovascular system. The heart nourishes the systemic circulation with blood at flow rate $q(t)$ with arterial pressure $P(t)$.

measurements (along with other pertinent clinical details such as patient age, presence or absence of valve disease, etc.). The Multi-parameter Intelligent Monitoring for Intensive Care II (MIMIC II) database [16] is the product of an initiative by the MIT Laboratory for Computational Physiology (LCP) to create a massive, temporal database to facilitate the research and development of an Advanced Patient Monitoring System. Currently, this database has physiologic waveform data from over 3500 ICU patients hospitalized at Beth Israel Deaconess Medical Center, Boston, USA.

From this database, we identified 120 patients with simultaneously available ABP waveforms (125-Hz sampled) and thermodilution CO measurements. Since MIMIC II data is collected in a far less controlled environment than a typical research laboratory setting, ABP waveforms are prone to corruption, causing CO estimators to generate bizarre outputs. To address this problem, an algorithm that identifies and rejects bad waveform segments is required.

1.2 Thesis goals

The research presented in this thesis aims to achieve the following:

- To study the principles of CO estimation from ABP waveforms and build a computational system that estimates CO using 11 of the established methods.
- To evaluate and compare the performance of the CO estimation methods on a large set clinical data from the MIMIC II database and determine whether the CO estimation is useful for clinical use.
- To design and evaluate an algorithm that quantifies ABP waveform quality.

1.3 Thesis outline

This thesis is divided into six chapters and two appendices.

Chapter 2, *Cardiac Output Estimation Theory*, explains the principles of the 11 different methods we study for CO estimation. Physiologic principles and theory from electrical

circuits are used whenever appropriate to provide intuition. Limitations of CO estimation are also discussed.

Chapter 3, *Signal Abnormality Indexing*, addresses the key issue of ABP waveform quality. CO estimation relies on a clean ABP waveform, in which pressure and temporal features may be reliably obtained. This chapter discusses the design and evaluation of an algorithm that flags poor quality ABP waveforms.

Chapter 4, *Evaluation Methods*, explains the computational system built to evaluate CO estimation, which involves database extraction, ABP waveform processing, CO estimator implementation, and performance evaluation.

Chapter 5, *Results and Discussion*, reports the performance of CO estimation. We discuss subset error analysis to determine the physiologic situations in which CO estimators are likely to be more erroneous.

Chapter 6, *Conclusions and Future Research*, summarizes the important findings from this research and suggests possible areas worthy of further exploration.

Appendix A presents a table summarizing the acronyms and mathematical notations used throughout this thesis. Appendix B contains input/output relations of important MATLAB source code to help elucidate Chapter 4.

Chapter 2

Cardiac Output Estimation Theory

In the cardiovascular system, the relationship between arterial blood pressure (ABP) and cardiac output (CO) is quite complex. Over a dozen methods of estimating flow from pressure have been proposed. Most of the methods operate at a beat-by-beat time resolution, calculating the stroke volume of each beat. Then, CO is calculated by multiplying stroke volume with heart rate. The bases of these methods are models of the systemic circulation.

Table 2.1 lists the 11 CO estimators studied in this thesis. (Several CO estimators are not studied because (1) the algorithms described in publications were unclear or (2) they are too similar to one of the 11 estimators in Table 2.1.) All expressions given in the table are proportional to CO. The proportionality constant encapsulates terms such as arterial compliance and peripheral resistance that are not obtainable from a given model. The first 5 methods are based on lumped-parameter circuit models of circulation. The next 4 are based upon distributed transmission line models. The last 2 are lumped circuit models with ability to produce instantaneous flow waveforms, which becomes CO when time-averaged.

Table 2.1: Cardiac output estimators

CO estimator	**CO** $= k \cdot$ **below**
Mean arterial pressure	P_m
Windkessel [5]	$P_p \cdot f$
Windkessel RC decay [4]	$\frac{P_m}{T} \cdot \ln \frac{P_s}{P_d}$
Herd [7]	$(P_m - P_d) \cdot f$
Liljestrand nonlinear compliance [12]	$\frac{P_p}{P_s + P_d} \cdot f$
Systolic area [19]	$A_s \cdot f$
Systolic area with correction [19, 10]	$\left(1 + \frac{T_s}{T_d}\right) A_s \cdot f$
Systolic area with corrected impedance [21]	$(163 + f - 0.48 \cdot P_m) \cdot A_s \cdot f$
Pressure root-mean-square—simplified form of [9]	$\sqrt{\langle (P(t) - P_m)^2 \rangle} \cdot f$
Godje nonlinear compliance [6]	complex formula
Wesseling Modelflow [20]	nonlinear, time-varying model

See Appendix A for notational explanations.

2.1 Lumped parameter methods

2.1.1 Mean arterial pressure

In the simplest model, the heart is represented as a current source and systemic circulation as a resistor (Figure 2-1). This circuit analogy is only appropriate for time-averaged flow, not pulsatile flow. Given mean arterial pressure and systemic resistance, CO may be computed via Ohm's law as follows:

$$Q = \frac{P_m}{R}$$

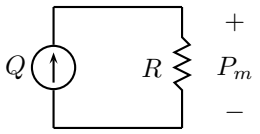

Figure 2-1: Mean arterial pressure P_m and cardiac output Q.

2.1.2 Windkessel model [5]

The arteries are capable of storing blood. Even with zero transmural pressure across the arterial walls, approximately 500ml of blood can reside inside the arterial system for a nominal person. At a mean arterial pressure of 100mmHg, 700ml of blood are in the arteries [13]. Therefore, it is sensible to represent the arteries as a capacitor (Figure 2-2). This model is the Windkessel model.

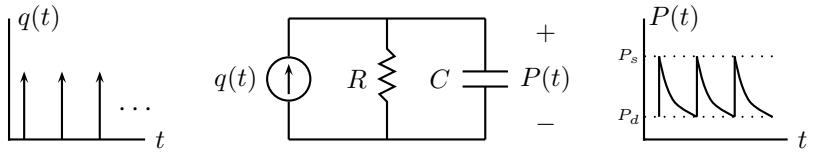

Figure 2-2: The Windkessel RC circuit model. The heart is modeled as a flow source $q(t)$ with impulse train ejections. Systemic circulation is modeled with arteriolar resistance R and arterial compliance C. The ABP waveform $P(t)$ generated has an infinitesimally short systolic duration followed by exponential decay during diastole.

One major "upgrade" in the Windkessel model is in its ability to capture the pulsatility of the cardiovascular system. The current source, now as an ideal pulsatile pump, generates a periodic impulse train, which gives rise to the ABP waveform $P(t)$. From circuit theory, it can be shown that in steady state, stroke volume is proportional to the amplitude of the ABP waveform ($P_s - P_d$) and arterial capacitance. Thus, CO is given as:

$$Q = C \cdot P_p \cdot f$$

2.1.3 Windkessel RC decay [4]

If the time constant τ of the Windkessel RC circuit model is known, then cardiac output may be computed in another way:

$$Q = \frac{P_m}{R} = C \cdot \frac{P_m}{RC} = C \cdot \frac{P_m}{\tau}$$

There are several methods to determine τ:

- Use the Windkessel idealization that ejection is instantaneous. This way, the entire cardiac cycle is in exponential decay from systolic to diastolic pressure. Mathematically,

  $$P_d = P_s e^{-T/\tau}$$

  where T is the beat period. Solving for τ, we obtain:

  $$\tau = \frac{T}{\ln \frac{P_s}{P_d}}$$

  Hence, the final CO expression:

  $$Q = C \cdot \frac{P_m}{T} \cdot \ln \frac{P_s}{P_d}$$

- Perform a least squares fit of an exponential decay to the diastole portion of the ABP waveform. Then, the best-fitted τ is obtained.

- Use a refined exponential fitting technique by Mukkamula et al. [14].

In this thesis, τ is obtained separately using the first two methods.

2.1.4 Herd [7]

The Herd method proposes that stroke volume is proportional to $P_m - P_d$. This methodology is based upon empirical evidence and no physiologic intuition is given [7].

2.1.5 Liljestrand nonlinear compliance [12]

Arterial capacitance is not constant but varies as a function of pressure. As arterial pressure increases, arterial walls stiffen, reducing capacitance. From the Windkessel model point of view, the Liljestrand and Zander method takes into account the nonlinearity using $C = \frac{k}{P_s + P_d}$ (Figure 2-3). Hence, CO becomes:

$$Q = \frac{k}{P_s + P_d} \cdot P_p \cdot f$$

2.2 Pressure-area methods

One major problem with lumped parameter models is that the arterial tree is really a distributed, not lumped system (Figure 2-4). In theory, the arterial tree could be more

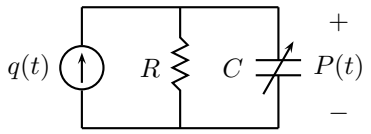

Figure 2-3: Windkessel model with nonlinear capacitor. Liljestrand and Zander propose that $C \propto (P_s + P_d)^{-1}$.

accurately modeled using the transmission line circuitry, which captures the distributed nature and associated effects such as impedance and wave reflections. Although none of the pressure-area methods are explicitly derived from transmission line circuit theory, the arterial tree is approached from a distributed system point of view.

2.2.1 Systolic area [19]

One key observation made from the distributed arterial tree is that stroke volume is proportional to the area under the systole region (A_s) of the ABP waveform (Figure 2-6). CO becomes:

$$Q = k \cdot A_s \cdot f$$

2.2.2 Systolic area with correction [19, 10]

First appearing in Warner et al. [19], a $(1 + T_s/T_d)$ correction factor was applied to the previous CO estimation method. This factor is probably compensating for the fact that the duration of systole, T_s, is not a negligible fraction of the beat period, thereby causing outflow from the capacitor to the resistor. The exact physiologic rationale is unexplained. CO estimate with this correction factor becomes:

$$Q = k \cdot \left(1 + \frac{T_s}{T_d}\right) A_s \cdot f$$

2.2.3 Systolic area with corrected impedance [21]

Wesseling et al. [21] introduced another correction factor based upon empirical evidence and optimal regression analysis. With the corrected impedance factor, CO becomes:

$$Q = k \cdot (163 + f - 0.48 \cdot P_m) \cdot A_s \cdot f$$

2.2.4 Pressure root-mean-square [9]

An adaption of LiDCO's CO method [9], stroke volume is thought to be proportional to the root-mean-square of each cycle in the ABP waveform. From AC circuit theory, root-mean-square of an AC voltage waveform is proportional to power. Thus, this method believes that stroke volume and AC power of the ABP waveform are linearly related. Thus, CO becomes:

$$Q = k \cdot \sqrt{\langle (P(t) - P_m)^2 \rangle} \cdot f = k \cdot \sigma(P(t)) \cdot f$$

Note that root-mean-square and standard deviation σ are numerically equivalent.

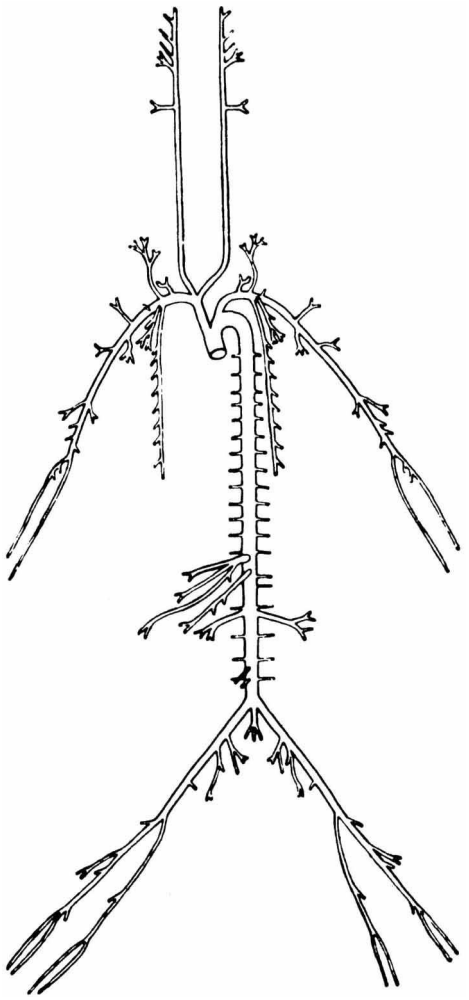

Figure 2-4: Arterial tree of a dog. In reality, the arterial tree is more accurately modeled by transmission lines rather than lumped parameter model. Figure adapted from [15].

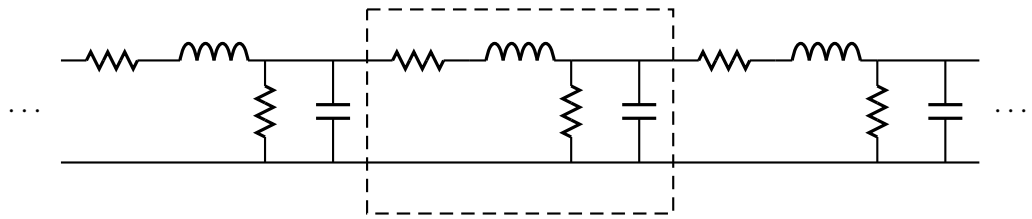

Figure 2-5: A transmission line circuit. The elementary component is enclosed by the dashed box. The transmission line is a series of elementary components. With the inductor-capacitor pairing, pulse wave propagation is generated.

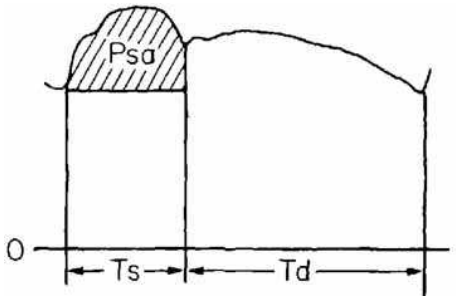

Figure 2-6: Pressure-area during systole. One cycle of the ABP waveform is shown. Stroke volume is believed to be proportional to the area of the shaded region. Figure adapted from [10].

2.3 Lumped-parameter, instantaneous flow methods

Two of the CO estimation methods investigated in this thesis use lumped parameter models to calculate the instantaneous pulsatile flow, $q(t)$, from ABP waveforms. Once $q(t)$ is obtained, then beat-to-beat CO is the time-averaged flow over a cardiac cycle:

$$Q = \frac{1}{T}\int_T q(t)dt$$

2.3.1 Godje nonlinear compliance [6]

Godje's cardiovascular system model is shown in Figure 2-7. Compared to the Windkessel model, an aortic impedance element, Z, is added, and the heart becomes a pressure source rather than a flow source. Also, arterial compliance is nonlinear. The expression for arterial compliance is optimized to minimize mean square error of the flow (derivation for the optimization is not given in the paper):

$$C = \frac{P_m^3}{R \cdot \langle dP(t)/dt \rangle} \cdot \frac{1}{3P_m P(t) - 3P_m^2 - P(t)^2}$$

Using Kirchhoff's current law, instantaneous flow is obtained:

$$q(t) = \frac{P(t)}{R} + C\frac{dP}{dt} = \frac{1}{R}\left(P(t) + \frac{P_m^3}{3P_m P(t) - 3P_m^2 - P(t)^2} \cdot \frac{dP(t)/dt}{\langle dP(t)/dt \rangle}\right)$$

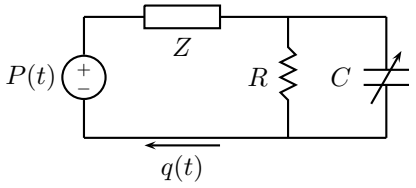

Figure 2-7: Godje model with nonlinear capacitance and aortic impedance terms.

2.3.2 Wesseling Modelflow [20]

Wesseling's modelflow method is one of the most complex (Figure 2-8). The circuit is similar to Godje's but with every circuit element becoming nonlinear. Aortic impedance is a function of arterial compliance; arterial compliance is a function of pressure; systemic resistance is a function of pressure divided by flow. The nonlinear relationship between C and $P(t)$ are based from Langewouters et al.'s [11] regressions.

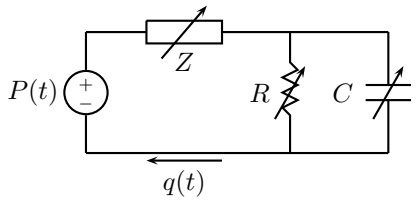

Figure 2-8: Wesseling's modelflow model.

2.4 Limitations of CO estimation

The 11 methods of estimating CO from ABP waveforms have several limitations. First, all methods require at least one calibration to obtain absolute CO values in liters per minute. Without calibration from a CO measurement such as thermodilution, one can only obtain relative estimates, which are still beneficial to the clinicians, especially if CO changes by a substantial fraction in a given patient.

The cardiovascular models used to estimate CO are vastly simplified from reality, even for the most complex ones. First, although the pressure-area under systole methods are based upon the distributed arterial tree, the theoretical foundations are not firmly established [19, 10]. It would be beneficial to derive an expression for CO from transmission line theory. Second, many of the methods assume that a central ABP waveform (such as one from the aorta) is used. Clinically, radial ABP waveforms are by far more popularly measured. Figure 2-9 shows that there is a substantial difference between ABP waveforms in aorta versus radial arteries, though there are models that attempt to estimate the aortic waveform using the radial artery waveform. Lastly, systolic area calculations require detecting the end of systole, which is completely nontrivial in radial ABP waveforms. In aortic ABP, the dicrotic notch signifies the end of systole. In radial ABP, the dicrotic notch is masked by wave reflections and high frequency signal attenuation.

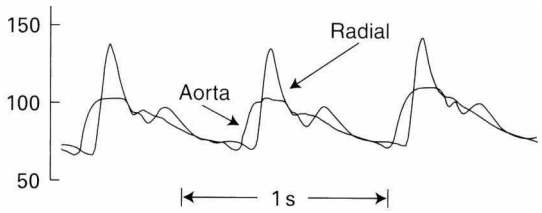

Figure 2-9: Pressure waveforms in aorta versus radial artery. Notice that systolic pressure in the radial artery tends to be higher than that of the aorta. Figure adapted from [15].

For several reasons, the more complex methods may perform worse than the simpler ones. First, due to corruption susceptibility of the ABP waveform, especially in a clinical setting, complex methods may falter if a particular ABP feature is corrupt. The simplest method, CO is proportional to mean arterial pressure, is by far most robust to noise because of its averaging nature. Second, the more complex methods have more circuit components. Wesseling's modelflow method determines the value of each component through ABP waveforms and regressions using age and gender. Regression lines were determined from a very small population (less than 50), which may not be representative of the entire human population. Therefore, modelflow may only perform well on patients with similar physiology to Wesseling's small study population.

A fundamental limitation of CO estimation performance is due to ABP waveform quality. Features and morphology of the ABP waveform need to be clean, especially for the more complex CO estimation methods. Thus, CO estimation is likely to fail in patients with intra-aortic balloon pumps, valve regurgitation diseases, and long-lasting arrhythmias such as atrial fibrillation.

Further discussion on the limitations of CO estimation can be found in an editorial by Lieshout and Wesseling [18].

Chapter 3

Signal Abnormality Indexing

3.1 Introduction

Cardiac output (CO) estimation from arterial blood pressure (ABP) waveforms rely on a clean ABP waveform, in which beat-to-beat features such as mean pressure, duration of systole, and beat period may be reliably obtained. Noisy, artifactual, damped, and irregular (not sinus rhythm) ABP waveforms may easily lead to bizarre CO estimates. Figures 3-1, 3-2, 3-3, 3-4 show examples of clinical ABP waveforms from MIMIC II in which CO estimates are likely to fail. Therefore, it is important to design an algorithm that can flag anomalous beats in the ABP waveform (Figure 3-4). We define a beat as *anomalous* when any feature in the beat becomes obscured. Median filtering helps to reduce some sporadic anomalies, but fails as anomalies become more frequent.

In this chapter, we present the signal abnormality index (SAI). The algorithm outputs at a beat-level time resolution and intelligently detects abnormal beats by imposing a series of constraints on physiologic, noise/artifact, and beat-to-beat variability. SAI does not distinguish between anomalies arising from physiologic disturbances such as an arrhythmia and non-physiologic phenomena such as noise.

The SAI algorithm was evaluated on clinical ABP waveforms of 120 patients from MIMIC II (see Section 1.1.3). Using the 120 records, we quantified the performance of the SAI algorithm in 3 ways: comparing the algorithm's performance to a human expert, analyzing the sensitivity of the algorithm's output, and determining whether cleaner waveform segments yield better CO estimates.

3.2 Methods

Figure 3-5 shows an overview of the SAI algorithm. First, a beat detection algorithm [22] marks the onset of each beat. The onset markers allow for feature extraction at beat-level resolution. For each beat, features such as heart rate, systolic blood pressure, diastolic blood pressure are obtained. Features are then evaluated by a series of abnormality criteria, which check for noise level, physiologic ranges, and beat-to-beat variations. The output of each abnormality criterion is binary, '0' for no flag (clean beat) and '1' for flag. Finally, the outputs of all abnormality criteria are combined via the logical OR operation.

Given an input ABP segment of n beats, the overall output (define as y) is a binary

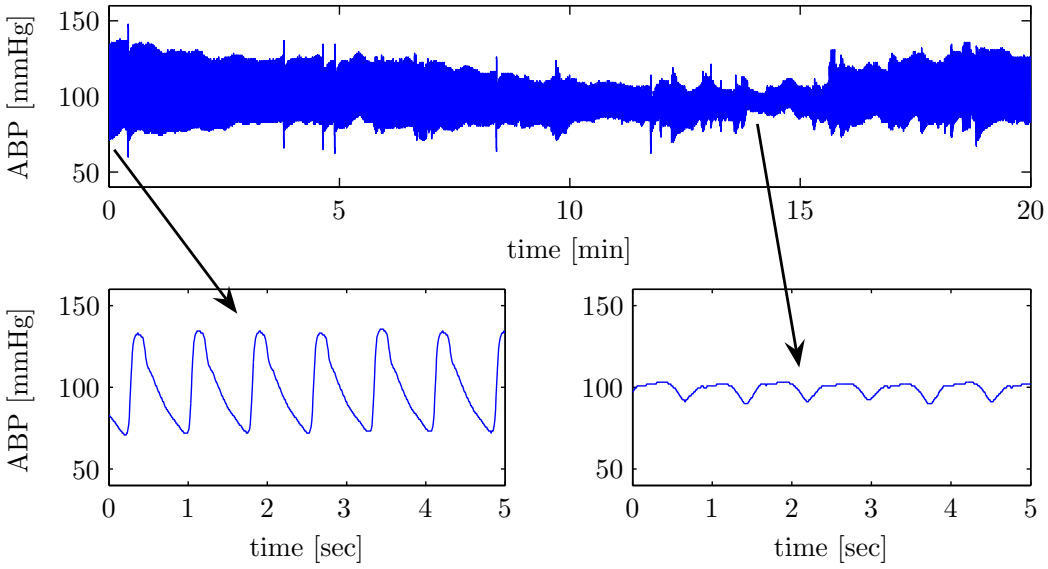

Figure 3-1: Damped ABP waveform. Top plot shows a 20 minute ABP waveform. Bottom-left plot is a zoom-in near the earlier part, and bottom-right plot is a zoom-in around the 14th minute. Damping caused the pulse pressure to decay from 60mmHg to 10mmHg.

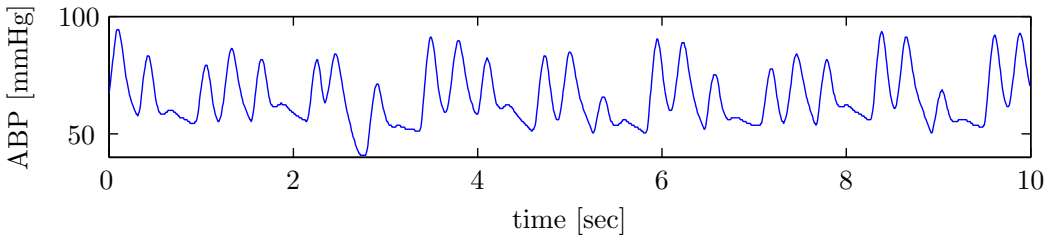

Figure 3-2: ABP waveform with disturbance. Beat detection becomes nontrivial and unpredictable here, giving rise to inaccurate CO estimates. (Upon closer examination of the patient record, this waveform segment was from a patient who had an 2-to-1 intra-aortic balloon pump, which generated the middle beat for each group of 3 beats shown.)

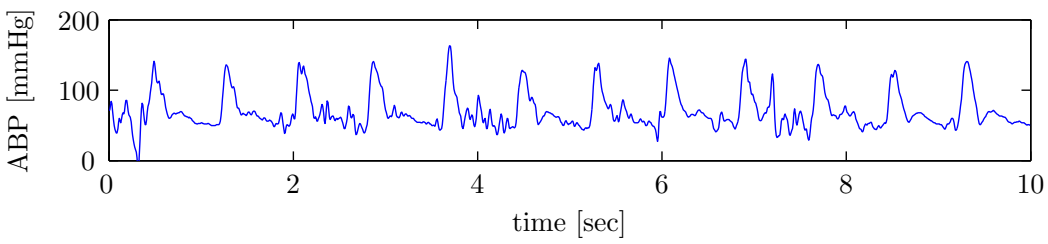

Figure 3-3: Noisy ABP waveform. Noisy beat-to-beat features give rise to inaccurate CO estimates, especially for the more complicated CO estimators.

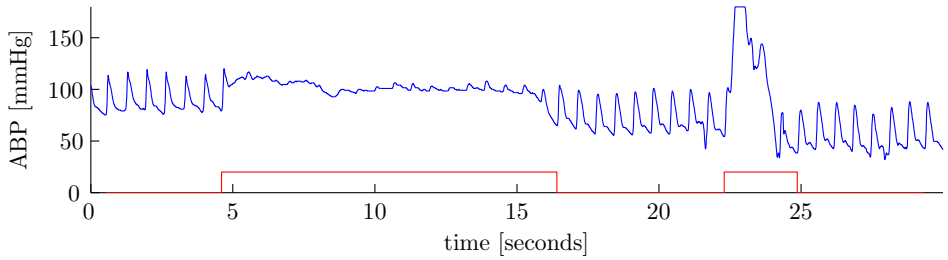

Figure 3-4: ABP waveform with artifacts. Corruption in the first 15 seconds is likely due to improper catheterization caused by movement. Corruption in 20-22 seconds is likely a motion artifact. Signal abnormality index (SAI) is shown on bottom, raising a flag in regions of abnormality.

sequence of length n. For the segment, a cumulative SAI (cSAI) is defined as

$$Y \equiv \text{fraction of flagged beats} = \frac{1}{n}\sum_{k=1}^{n} y[k]$$

where $y[k]$ is the SAI of the k-th beat. cSAI, with a continuous domain of $0 \leq Y \leq 1$, is a useful measure of the abnormality of an entire waveform segment. (e.g. a segment of 50 beats with 4 flagged would yield a cSAI of 0.08.)

The rest of this section explains several components of the SAI in detail and proposes methods for algorithm evaluation.

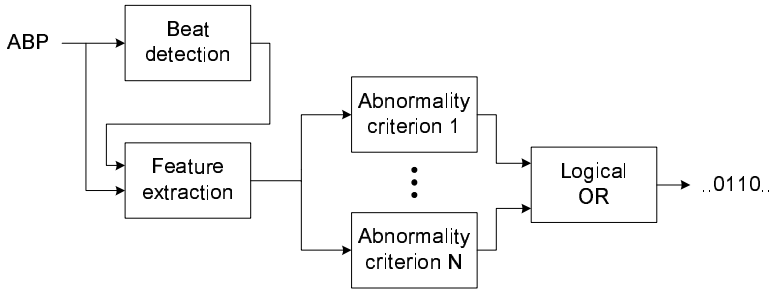

Figure 3-5: SAI block diagram. Input is an ABP waveform. Output is a binary string, assigning a value (no flag=0, flag=1) to each beat in the ABP waveform.

3.2.1 Feature extraction

The feature extraction algorithm obtains a set of features shown in Table 3.1. For each beat, P_s and P_d are the local minimum and maximum around the pressure onset point. P_m is the average pressure between adjacent onsets. T is the time difference between adjacent onsets. Noise level is defined as the average of all negative slopes in each beat.

3.2.2 Abnormality indexing

With blood pressure features available, the SAI algorithm is ready to interpret them. Table 3.2 lists the criteria for flagging a beat.

Table 3.1: ABP features

Feature	Description
P_s	Systolic blood pressure
P_d	Diastolic blood pressure
P_p	Pulse pressure ($P_s - P_d$)
P_m	Mean arterial pressure
T	Duration of each beat
f	Heart rate ($60/T$)
w	noise: mean of negative slopes

Table 3.2: SAI logic

Feature	Abnormality criteria
P_s	$P_s > 300$ mmHg
P_d	$P_d < 20$ mmHg
P_m	$P_m < 30$ or $P_m > 200$ mmHg
f	$f < 20$ or $f > 200$ bpm
P_p	$P_p < 20$ mmHg
w	$w < -40$ mmHg/100ms
$P_s[k] - P_s[k-1]$	$\lvert\Delta P_s\rvert > 20$ mmHg
$P_d[k] - P_d[k-1]$	$\lvert\Delta P_d\rvert > 20$ mmHg
$T[k] - T[k-1]$	$\lvert\Delta T\rvert > 2/3$ sec

The first 5 criteria in Table 3.2 impose bounds on the physiologic ranges of each feature. For example, any beat with a diastolic pressure of less than 20mmHg is flagged.

The 6th criterion is the noise detector. With high frequency noise, there will be large negative slopes in the waveform. Based upon this observation and by inspecting ABP data, we decided that any beat with a mean negative slope less than -40mmHg/100ms is flagged. Note that this noise detector is not useful for identifying low frequency noise such as baseline wander.

The final 3 criteria compare ABP features between adjacent beats. Large sudden changes in beat-to-beat features are likely indications of abnormality. For example, if the $(k-1)$-th systolic pressure and the k-th systolic pressure differs more than 20mmHg, then the k-th beat is flagged.

3.2.3 Algorithm evaluation

Using 120 patient records from the MIMIC II database, the SAI algorithm was evaluated in 3 ways:

1. Compare the algorithm's performance to a human expert in detecting anomalies in ABP waveform segments. Ideally, the algorithm should be in perfect concordance with the human.

2. Analyze the sensitivity of algorithm's output to perturbations of each threshold parameter in Table 3.2. A robust algorithm would be relatively insensitive to such perturbations.

3. Determine whether cleaner waveform segments, as indicated by low cSAI values, yield better CO estimates.

In comparing to a human expert annotator, 246 ABP segments were randomly selected, each 10 seconds long. For each segment, the SAI algorithm outputs '1' if any beat is flagged as abnormal, '0' otherwise. Similarly, the human identifies any abnormality and classifies each segment using the following convention:

−− No irregularity—regular, homogeneous beats with negligible artifacts and noise.

−+ Minor irregularity—clean waveform with minor timing irregularity of beats and/or minor artifacts. Key morphologic features are still clearly identifiable.

+− Irregularity present—all beats similar, but one beat stands out from others with timing or shape, and/or artifact present obscuring a portion of a beat.

++ Major irregularity present—more than one beat patently dissimilar from other beats, and/or artifact present completely obscuring key features of beats.

Notice that human annotations have 2 gray zones (−+ and +−), which are used when the waveform's abnormality is not completely obvious.

For sensitivity analysis, the abnormality criteria are tested independently of each other. A parameter value in Table 3.2 is perturbed while all other abnormality criteria are not applied. We observe the impact on cSAI across the entire study population, which includes over 30 million beats. Sensitivity is defined as follows:

$$\text{Sensitivity} \equiv \left.\frac{dY}{d\hat{\theta}}\right|_{\hat{\theta}=1}$$

where Y is the cSAI and $\hat{\theta}$ is the normalized parameter value. Normalization allows for sensitivity comparison between different abnormality criteria.

We examine the performance of 3 CO estimation algorithms (Table 3.3) as a function of cSAI. For our study population, a 1-minute ABP segment is extracted at the time of each TCO measurement. Estimated CO and cSAI are obtained for each 1-min ABP segment. For the entire population, the error metric is $\sigma(CO - TCO)$, the standard deviation of the difference between estimated CO and TCO. The error is evaluated as a function of cSAI. We begin the experiment by examining σ of the entire population with no discrimination due to cSAI. Then, 1-min segments with high cSAI values (poor waveform quality) are progressively eliminated. The goal is to determine whether CO estimation error decreases for cleaner waveforms.

Table 3.3: CO estimators taken from Table 2.1.

CO estimator	**CO** $= k \cdot$ **below**
Mean arterial pressure	P_m
Windkessel	$P_p \cdot f$
Liljestrand nonlinear compliance	$\frac{P_p}{P_s+P_d} \cdot f$

3.3 Results

3.3.1 SAI versus human

Table 3.4 shows the distribution of the 246 comparisons of SAI versus a clinician (ATR). Note that SAI performance is worse in the two grays zones ($-+$ and $+-$). However, only 22% of data fall into these categories. Table 3.5 lists important statistics derived from the distribution, both exclusive (3rd column) and inclusive (4th column) of the gray zones.

Table 3.4: SAI versus human: distribution

SAI					
1	14	13	9	37	
0	142	26	5	0	
	$--$	$-+$	$+-$	$++$	human

Distribution of the 246 ABP waveform segments. SAI key: 0 no flag, 1 flag. Human key: $--$ no flag, $-+$ probably no flag, $+-$ probably flag, $++$ flag

Table 3.5: SAI versus human: statistical summary

PPV	$P(+\|1)$	0.73	0.63
NPV	$P(-\|0)$	1	0.97
Sensitivity	$P(1\|+)$	1	0.90
Specificity	$P(0\|-)$	0.91	0.86

3rd column excludes gray zones, 4th column includes gray zones. PPV=positive predictive value, NPV=negative predictive value, $P(*|*)$ are conditional probability notations for PPV, NPV, etc.

3.3.2 Sensitivity analysis

Figure 3-6 plots cSAI as a function of 3 abnormality criteria. Notice that each criterion flags only a small fraction of beats, and the slope of the curves are not steep but also nonzero at $\hat{\theta} = 1$. Table 3.6 lists the sensitivity of every parameter. The results indicate that our study population had no waveform with $P_s > 300$mmHg or $P_m > 200$mmHg.

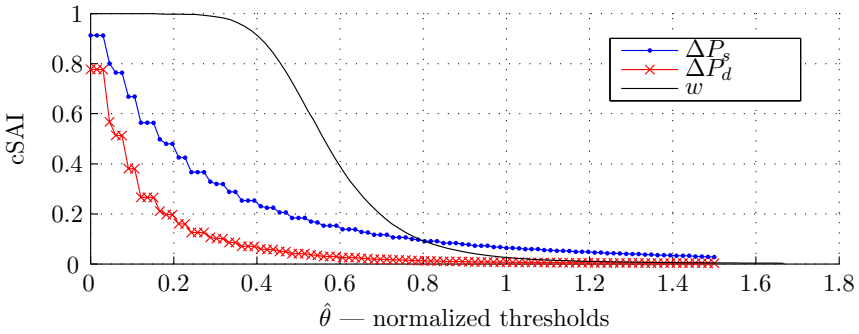

Figure 3-6: Perturbations to abnormality criteria. cSAI as a function of 3 parameters perturbations is shown. Sensitivity is defined to be the slope of each curve at $\hat{\theta} = 1$.

Table 3.6: SAI sensitivity

Feature	θ_0	$Y(\theta_0)$	|Sensitivity|
P_s	300	0	0
P_d	30	.010	.003
$P_{m,min}$	30	.007	.007
$P_{m,max}$	200	0	0
f_{min}	20	.001	.001
f_{max}	200	.047	.180
P_p	20	.028	.092
w	-4	.027	.160
$P_s[k] - P_s[k-1]$	20	.064	.080
$P_d[k] - P_d[k-1]$	20	.007	.013
$T[k] - T[k-1]$	0.7	.017	.033

3.3.3 Cardiac output estimation error

Figure 3-7 plots CO estimation error as a function of maximum accepted cSAI. Errors decrease for lower cSAI (cleaner waveform) values. For the Liljestrand algorithm, an error reduction of 30% is obtained. The mean pressure estimation algorithm is most robust to noise, as evidenced by its relatively flat line. This robustness is expected because of the simplicity and averaging nature of the mean pressure algorithm.

3.4 Discussion and conclusions

Evaluating the performance of the SAI algorithm is nontrivial, primarily because of a lack in the quantitative definition of an 'abnormal' beat of an ABP waveform. Consequently, there is no established gold standard to compare against. Furthermore, the definition of abnormality can be application dependent. For example, beat quality needs to be higher for CO estimation than for mean pressure tracking because more features derived from each beat are used for the former. From Figure 3-7, a maximum accepted cSAI level of 0.5 can be routinely used for CO estimation purposes. At $cSAI = 0.5$, only 10% of the poorest ABP data have been removed, CO estimation error has been substantially reduced, and the data quantity does not change very rapidly around this point.

From the sensitivity analysis, two abnormality criteria do nothing and have sensitivity of 0. Therefore, for our study population, they can be removed. Of the remaining criteria, pairwise correlation studies can be performed in the future to identify any redundant criteria.

In conclusion, we have presented an algorithm that detects anomalies in the ABP waveform. The SAI algorithm is in close agreement with a human expert (Table 3.5), is robust (Table 3.6), and has proven its effectiveness in its ability to select clean ABP waveforms to improve CO estimation.

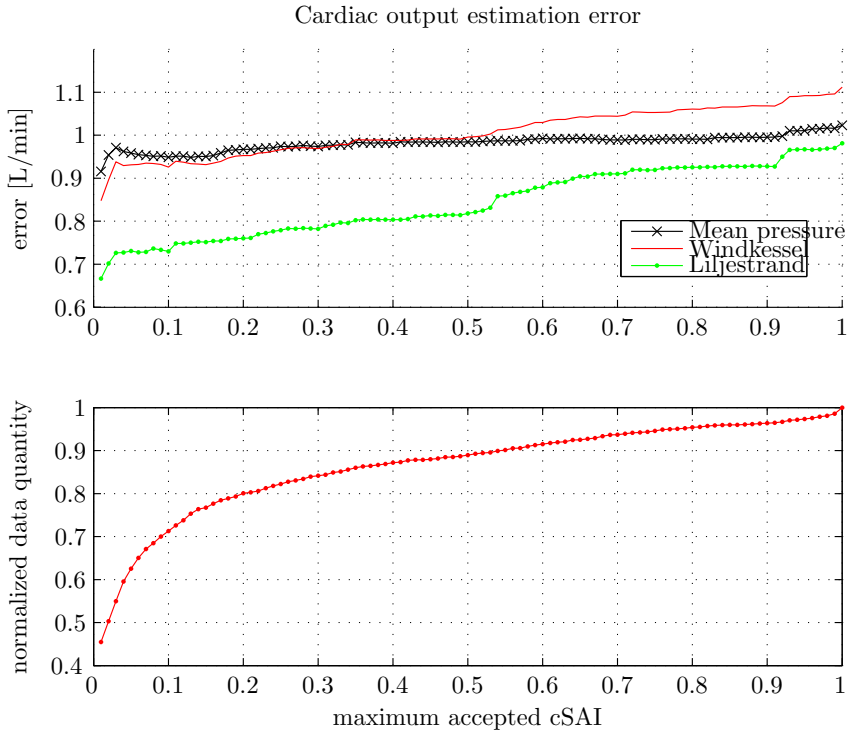

Figure 3-7: CO estimation error as a function of maximum accepted cSAI. Bottom plot shows that the amount of data also decreases as we restrict ourselves to cleaner waveforms.

Chapter 4

Evaluation Methods

Evaluating the performance of cardiac output (CO) estimation requires obtaining the following signals:

- **A set of ABP waveforms** as input for the CO estimators. In order to capture the intra-beat waveform morphology, sampling rate of ABP needs to be sufficiently high (greater than 60Hz).
- **A set of gold-standard CO measurements** to compare with estimated CO. Each measurement must be available simultaneously to ABP waveform recordings. We will use thermodilution CO (TCO) measurements as gold-standard. It is well known that TCO has errors itself [17]. Thus, by comparing estimated CO to TCO, our results are limited by TCO's accuracy.

The signals will be processed by the following systems:

- **A data extraction system** to identify suitable ABP waveforms and TCO measurements for analysis.
- **A CO estimation system** to accurately and efficiently implement each CO estimation algorithm. Ideally, we obtain the 11 algorithms from the original creators and use their exact implementation. However, this is impractical in many ways. Hence, we peruse their publications and mimic their methods as closely as possible.
- **A comparison system** to output the error between each estimated CO and TCO. This system may seem trivial, involving a simple subtraction. However, a major problem is that all CO estimates are given in relative units (Table 2.1). Therefore, we must establish suitable calibration methods before performing comparisons. We also design a scheme comparing percentage changes in estimated CO and TCO. This scheme does not require calibration.
- **An error analysis system** to report the performance of CO estimates across the entire study population. We also explore the physiologic conditions in which CO estimators are likely to fail. Using these analyses, our goals are (1) to determine whether CO estimates are reliable enough for clinical use, and (2) to investigate the possibility of improving CO estimates.

Figure 4-1 presents a high-level flow chart showing the connectivity between the signals and systems outlined above. This chapter discusses each component in detail.

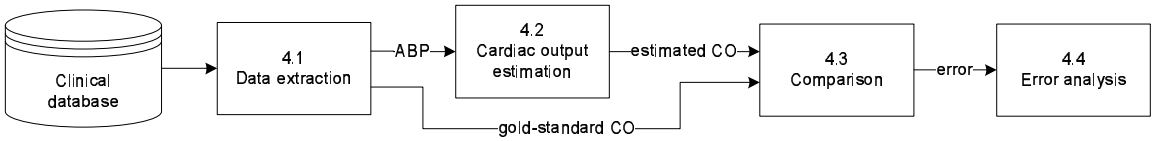

Figure 4-1: A system for evaluating CO estimation performance.

4.1 Data extraction

Relevant source code: `wavex.m`, `trendex.m` [1]
As described in Chapter 1, the clinical database we use is MIMIC II, which contains physiologic waveform data from over 3500 ICU patients hospitalized at Beth Israel Deaconess Medical Center, Boston, USA. From this database, we identified 120 patients with simultaneously available ABP waveforms and TCO measurements. The ABP waveforms are measured radially and stored as 8-bit quantized data with a temporal resolution of 125Hz. TCO is measured intermittently with a temporal resolution of 1 minute.

4.2 Implementation of CO estimators

With appropriate ABP waveforms extracted, we are now ready to make CO estimates. Figure 4-2 presents the flow chart showing the transformation of ABP into beat-by-beat CO. The first step is to detect beats in the ABP waveform. For each beat, various features such as instantaneous heart rate, systolic blood pressure, and pulse pressure are extracted. Given the features, the CO algorithms output CO estimates. The signal abnormality indexer identifies abnormal beats and eliminates them. Finally, we apply a low-pass filter and eliminate fluctuations in CO estimates caused by beat-to-beat variations. The rest of this section discusses each major block of the CO estimation system in detail.

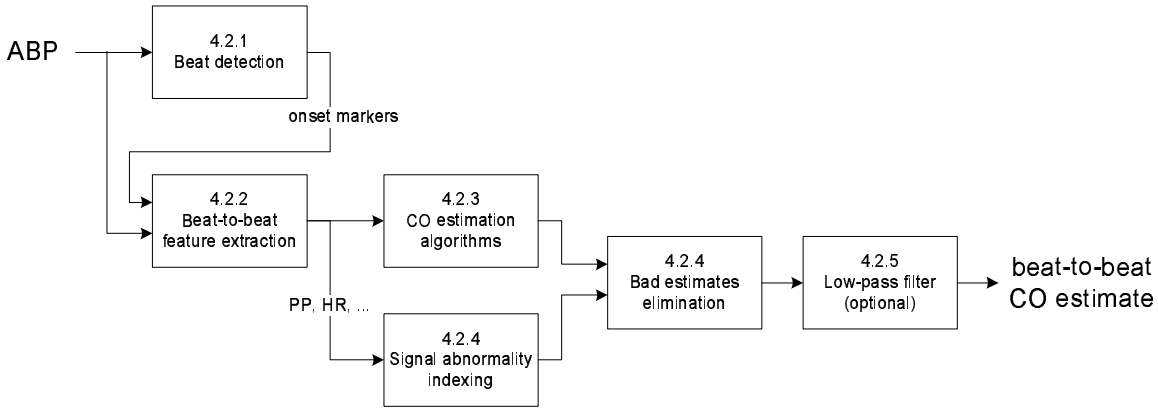

Figure 4-2: Data flow diagram for CO estimation.

4.2.1 ABP beat detection

Relevant source code: `wabp.m`
The beat detection system segments the ABP waveform into individual beats. The process

[1] See Appendix B for MATLAB source code descriptions.

is essential in extracting ABP features. We adopt an algorithm designed by Zong et al. [22] that robustly detects the onset of each beat in the ABP waveform. The basis of Zong's onset detection algorithm is the slope sum function (SSF), which amplifies the rising part of each beat (Figure 4-3). More details can be found in their paper.

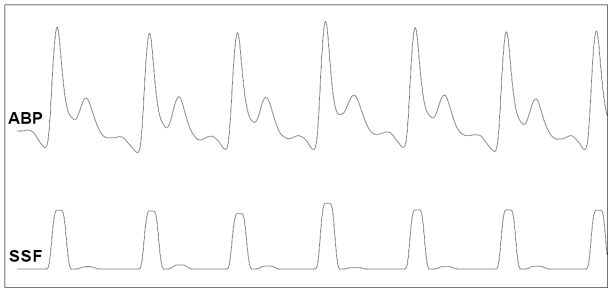

Figure 4-3: The slope sum function (SSF). It aids in onset detection. Figure adapted from [22].

4.2.2 ABP feature extraction

Relevant source code: `abpfeature.m`
After segmenting the ABP waveform into individual beats, we extract useful features from each beat. The complete set of extracted features is listed in Table 4.1.

Table 4.1: ABP features

Feature	Description	Units
P_s	Systolic blood pressure	mmHg
P_d	Diastolic blood pressure	mmHg
P_p	Pulse pressure ($P_s - P_d$)	mmHg
P_m	Mean arterial pressure	mmHg
A_s	pressure area during systole (2 methods)	mmHg·sec
w	mean of negative slopes (for noise detection)	mmHg/sec
T	Duration of each beat	sec
T_s	Duration of systole (2 methods)	sec
T_d	Duration of diastole ($T - T_s$)	sec

Figure 4-4 shows the identification of P_s, P_d, and P_p. P_s is the local maximum within a time window following each onset. Likewise, P_d is the local minimum within a window before each onset. P_p is the difference between P_s and P_d. P_m is the average of all pressure samples between adjacent onsets. T is the time difference between adjacent onsets. Noise level is defined as the average of all negative slopes in each beat.

As described in Chapter 2, many CO estimators require the detection of end-of-systole. End-of-systole's defining feature in the aortic pressure waveform is the dicrotic notch, marking the time in which the aortic valve closes (Figure 4-5). Unfortunately, wave reflections and high frequency signal attenuation in the radial arteries completely mask the dicrotic notch. However, publications often mistakenly associate the second peak of each beat as the dicrotic notch. The second peak is not the dicrotic notch but a reflected wave.

This nontriviality in end-of-systole detection lead us to employ two techniques to approximate end-of-systole, the RR method and the "first zero slope" (FZS) method. The

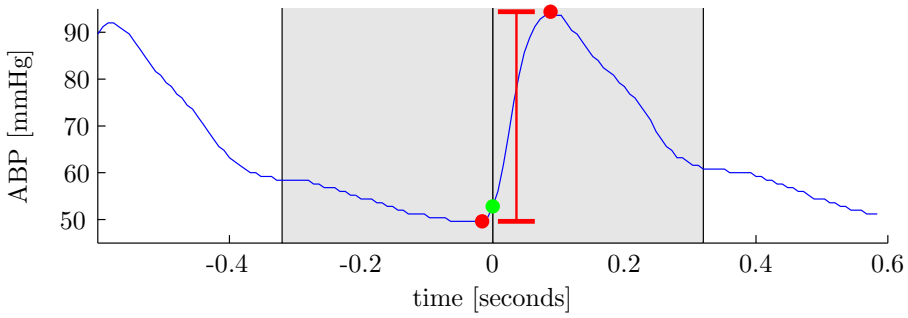

Figure 4-4: P_s, P_d, and P_p detection. The light dot marks the onset. The darker dots are P_s and P_d. The line segment marks P_p. The shaded areas are the two search windows for P_s and P_d.

RR method uses a result from electrocardiography. QT-interval duration is approximated as $0.3\sqrt{\text{RR interval}}$ [1], where RR-interval is measured in seconds. Intuitively, the QT fraction becomes smaller as the duration of a cardiac cycle lengthens. We approximate that the RR-interval equals the beat period. The QT-interval is the duration from electrical depolarization to repolarization of the ventricles. Therefore, for a normal healthy heart, we approximate the QT-interval and systolic ABP duration to be very similar. From Figure 4-5, these approximations are reasonable. Hence, $T_s = 0.3\sqrt{T}$. For the FZS method, we find the first time following P_s that the slope of ABP becomes 0. Preliminary testing showed that while the 2 methods may indicate significantly different end-of-systole times (Figure 4-6), both offered very similar results in terms of CO estimation performance.

The main purpose for end-of-systole detection is in calculating the area under ABP during systole of each beat. Figure 4-6 shows end-of-systole and systolic area.

$$A_s = \int_{T_s} (P(t) - P_d)dt$$

4.2.3 CO estimator implementation

Relevant source code: `est0<num>_<title>.m`
The first 9 CO estimators in Table 2.1 take features of the ABP waveform as input. Simple arithmetic operations are applied to produce beat-to-beat CO estimates. The last 2 estimators use beat-to-beat features and the raw ABP waveform. Differential equations are used to produce a flow waveform. Then, we integrate the flow waveform over the systolic duration to produce CO estimates.

4.2.4 Signal quality and bad beats elimination

Relevant source code: `jSQI.m, estimateCO.m`
Quality of the ABP waveform is essential in determining the performance of CO estimators. Noisy, artifactual, damped, and irregular (not sinus rhythm) ABP waveforms may easily lead to bizarre CO estimates. Figures 3-1, 3-4, 3-2, 3-3 from Chapter 3 show examples of ABP waveforms from MIMIC II in which CO estimates are likely to fail. In Chapter 3, we presented the SAI algorithm to flag abnormal beats in the ABP waveform. Flagged beats

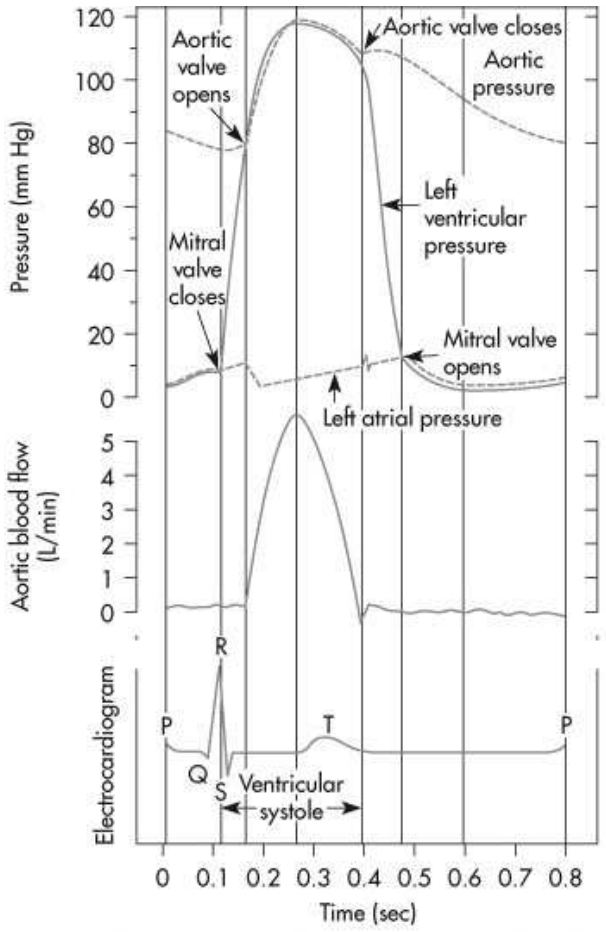

Figure 4-5: The cardiac cycle. Duration of systole can be approximated by the QT-interval duration. Figure adapted from [2].

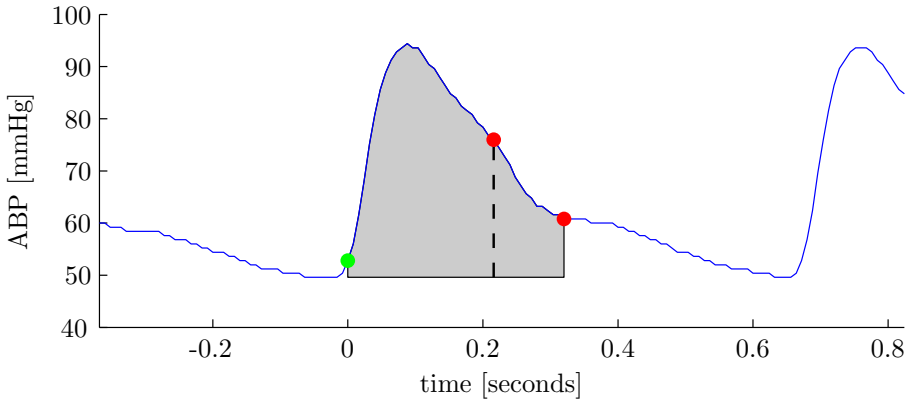

Figure 4-6: End of systole and systolic area. The light dot marks the onset. End of systole by the RR method is the earlier dark dot and by the FZS method is the later dark dot. The shaded area is the systolic area.

do not participate in CO estimation. Also, if a substantial percentage of beats are flagged in a given segment, the entire segment is excluded from CO estimation.

4.2.5 Running-average LPF to reduce beat-to-beat fluctuations

Relevant source code: `estimateCO.m`
Stroke volume varies on a beat to beat basis due to varying filling pressures caused by respiration. This phenomena occurs in every individual albeit in different magnitudes. For continuous tracking of CO, we would have beat-to-beat fluctuations if we simply apply CO estimation methods to each beat (Figure 4-7). Also, CO is a quantity more meaningful on the time scale of minutes rather than individual beats. Therefore, we apply a running-average low pass filter with a window of at least 10 seconds on all features extracted from the ABP, thereby obtaining an averaged stroke volume (hence CO) with much less inter-beat variability.

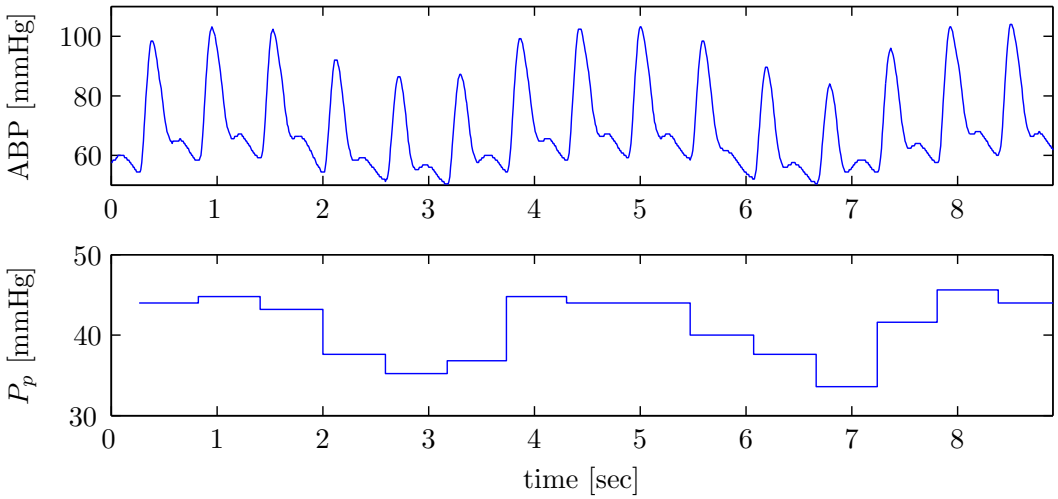

Figure 4-7: Beat-to-beat variability in ABP waveform due to respiration. P_p varies between 35 and 45mmHg, which can cause beat-to-beat CO estimates to have 25% fluctuations.

4.3 Comparing estimated CO to gold-standard CO

Relevant source code: `evco.m`
The goal of the comparison system is to report errors between estimated CO and gold-standard CO (thermodilution CO in our study). Let's define x as the estimated CO produced by one algorithm and r as the corresponding TCO measurement. Then, error is defined as:

$$e = x - r$$

There are two important complications that underly a seemingly simple subtraction:

- For each r, there are many beat-to-beat values of x. We need to average x over a suitable window.
- As shown in Table 2.1, CO estimates are in relative units. Thus, before comparing to TCO in units of liters per minute, we need perform a calibration in order to determine

the proportionality constant k.

Large percentage rises or drops in CO are of clinical interest. We devise a method to report the accuracy of CO estimates in determining percentage changes without calibration.

4.3.1 Averaging beat-to-beat CO estimates

In MIMIC II, TCO measurements are recorded with a 1-minute temporal resolution. Therefore, it is sensible to take the average CO estimate over the 1-minute window immediately preceding the TCO measurement. Figure 4-8 shows that a 1-minute averaged CO estimate is indeed robust to beat-to-beat fluctuations. Mathematically, our averaged CO estimate becomes:

$$x = \frac{1}{N} \sum_{k=T-N+1}^{T} a[k]$$

where $a[k]$ is CO estimate at the k-th beat, $a[T]$ is the CO estimate closest to the TCO measurement, N is the number of beats in the 1-minute window prior to the TCO measurement.

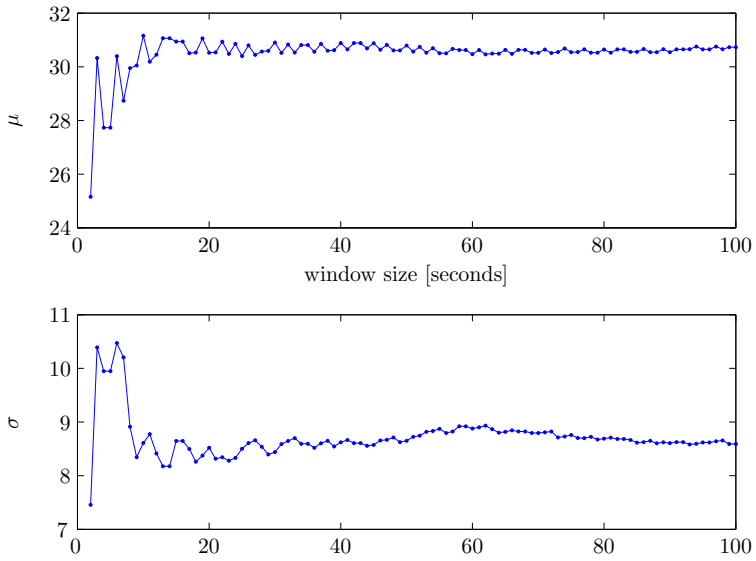

Figure 4-8: Window size for averaging CO estimates. Mean and standard deviation of a CO estimate (relative units) are shown as a function of window size. Notice that the two trends reach steady state after 10 seconds, suggesting that a minimum averaging window of 10 seconds is required in order to avoid beat-to-beat fluctuations.

4.3.2 Calibration techniques

For each patient, we calibrate each estimator in 3 ways (denoted as C1, C2, C3), each tailoring towards a different use model. In two of the calibration methods, we use a vector-based approach. For a patient with N TCO measurements, we construct an N-dimensional column vector, with one dimension for each measurement:

Reference CO (TCO): $\boldsymbol{r} = \begin{bmatrix} r_1 & r_2 & \cdots & r_N \end{bmatrix}'$
Uncalibrated estimate: $\boldsymbol{x} = \begin{bmatrix} x_1 & x_2 & \cdots & x_N \end{bmatrix}'$
Calibrated estimate: $\boldsymbol{q} = k\boldsymbol{x}$

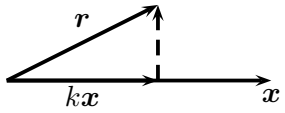

Figure 4-9: Vector visualization of TCO and estimated CO. For C1, we choose k to minimize error (magnitude of the dashed vector).

C1: Optimal single k. We choose a single constant k to minimize the mean square error. Using linear algebra, the optimal k is given as:

$$k = \frac{\boldsymbol{r}'\boldsymbol{x}}{\boldsymbol{x}'\boldsymbol{x}} \tag{C1}$$

C2: Optimal previous k. C1 calibration is useful in obtaining a lower bound of error for each estimator. However, C1 is noncausal and hence unsuitable in a live clinical setting. Therefore, for online estimation, we update our optimal k using previous data points. For the i-th k, we calibrate using the previous $(i-1)$-dimensional vector:

$$k_i = \frac{\boldsymbol{r}'_{i-1}\boldsymbol{x}_{i-1}}{\boldsymbol{x}'_{i-1}\boldsymbol{x}_{i-1}} \tag{C2}$$

Now the calibrated estimate becomes:

$$\boldsymbol{q} = \begin{bmatrix} k_1x_1 & k_2x_2 & \cdots & k_Nx_N \end{bmatrix}'$$

C3: First point single k. TCO measurements are usually taken very infrequently. Therefore, it is also useful to know the estimator performance by calibrating only to the first TCO measurement:

$$k = \frac{r_1}{x_1} \tag{C3}$$

The most prominent problem for C3 calibration: if x_1 is unusually noisy, producing an absurd calibration constant, the rest of CO estimates will be strongly affected. Consider the example: $\boldsymbol{x} = [20\ 50\ 20\ 30\ 40]$ and $\boldsymbol{r} = [1\ 5\ 2\ 3\ 4]$ L/min. Clearly, a good calibration constant would be $k = 0.1$, but the C3 method would yield $k = 0.05$.

4.3.3 Relative CO estimation

Outside of the ICU setting, invasive measurements of CO are likely unavailable; thus, we cannot calibrate to produce an absolute CO estimate. However, it would still be useful to know percentage changes in CO, especially if the changes are significant. For example, if the true CO decreased by 50%, we would like to know if the estimated CO has decreased by a similar percentage.

For each of the 120 patients, we search for the pair of TCO measurements with the largest difference in value. Then, the corresponding percentage change in the estimated CO

(Δx) and TCO (Δr) are compared. Mathematically:

$$\Delta r = \begin{cases} \left(\frac{r[i_{max}]}{r[i_{min}]} - 1\right) \times 100 & \text{if } t[i_{max}] > t[i_{min}] \\ \left(\frac{r[i_{min}]}{r[i_{max}]} - 1\right) \times 100 & \text{if } t[i_{max}] < t[i_{min}] \end{cases}$$

$$\Delta x = \begin{cases} \left(\frac{x[i_{max}]}{x[i_{min}]} - 1\right) \times 100 & \text{if } t[i_{max}] > t[i_{min}] \\ \left(\frac{x[i_{min}]}{x[i_{max}]} - 1\right) \times 100 & \text{if } t[i_{max}] < t[i_{min}] \end{cases}$$

where i_{max} is the index in which maximum TCO occurs, and correspondingly for i_{min}.

4.4 Error analysis

In the previous section, we established methods to obtain the error between each TCO measurement and estimated CO. Across the entire study population, for each CO estimator, we have an error *distribution*. In clinical literature, the most popular representation of error distributions is the Bland-Altman plot [3]. Figure 4-10 shows an example. The horizontal axis is the average of TCO and estimated CO. The vertical axis is the error. The major advantage of such a plot is that it enables one to see whether there's any correlation between the error and the averaged CO. For example, if error becomes substantial for high CO, then the estimated CO should not be trusted whenever it gives a high CO value.

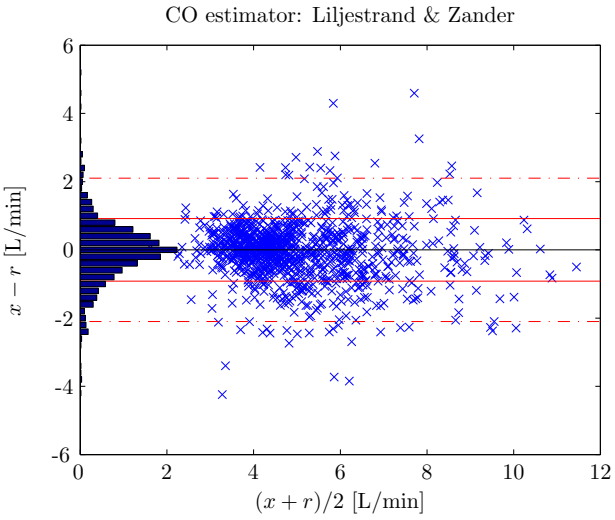

Figure 4-10: A sample Bland-Altman plot. The error histogram is shown on the left. The solid lines show 1 SD bounds, and the dashed lines show 95% confidence intervals.

With the aid of Bland-Altman plots, we present the performance of each CO estimator in the following ways:

CO estimation error. We report the 1SD and 95% confidence interval of the error distribution. If the error distribution is Gaussian, the numerical values for the 95% confidence interval and 2SD coincide.

k-variability. A good CO estimator should have a calibration constant (k) with low

variability across different patients. For example, if one ideal CO estimator has $k = 5 \pm 0.01$ for all of the 120 patients, then we can assume $k = 5$ and obtain the absolute CO estimate for any patient. However, if $k = 5 \pm 5$, then calibration is necessary for each patient. Mathematically, we quantify k-variability as:

$$k\text{-variability} = \frac{\text{SD of } k \text{ for the study population}}{\text{mean of } k \text{ for the study population}} = \frac{\sigma(k)}{\mu(k)}$$

Division by $\mu(k)$ enables us to compare the variability of k among different CO estimators. A k-variability of 0.1 would mean that the k fluctuates by 10% around the mean.

***CO*-variability.** A good CO estimator should produce beat-to-beat CO estimates with variability on the order of stroke volume and heart rate variability. It is undesirable for the stroke volumes to fluctuate beyond physiologically plausible ranges from beat-to-beat. *CO*-variability is measured for each 1-minute ABP waveform in which we obtain beat-to-beat CO estimates (no LPF is applied here). We assume that the physiological state is stable (e.g. average CO is constant) over the 1-minute window. Similar to k-variability, *CO*-variability is defined mathematically as:

$$CO\text{-variability} = \frac{\text{SD of } CO \text{ for a 1-min ABP waveform}}{\text{mean of } CO \text{ for a 1-min ABP waveform}} = \frac{\sigma(q)}{\mu(q)}$$

For each CO estimator, we report the average *CO*-variability over the entire study population. Because of the division by $\mu(CO)$, calibration is not necessary to determine *CO*-variability.

Relative CO estimation error. A good CO estimator, when uncalibrated, should still agree with TCO in terms of percentage increases and decreases. As discussed in Section 4.3.3, for each patient we identify the pair of data points with most significant change in TCO and compare it to the corresponding estimated CO. Figure 4-11 shows an example of relative CO estimation performance. For each CO estimator, we report the 1SD of the error distribution between percentage changes in estimated CO and TCO. We also report the performance of detecting directional changes, defined as:

$$P(+|+) = \text{probability of an increase in estimated CO given an increase in TCO}$$

$$P(-|-) = \text{probability of an decrease in estimated CO given an decrease in TCO}$$

Subset error analysis. A CO estimator may perform better in certain physiologic conditions than others. In subset error analysis, we show interesting plots of CO estimation error as a function of ABP features such as heart rate and mean arterial pressure. For example, a possible discovery would be that one CO estimator performs worse in high heart rates than low heart rates.

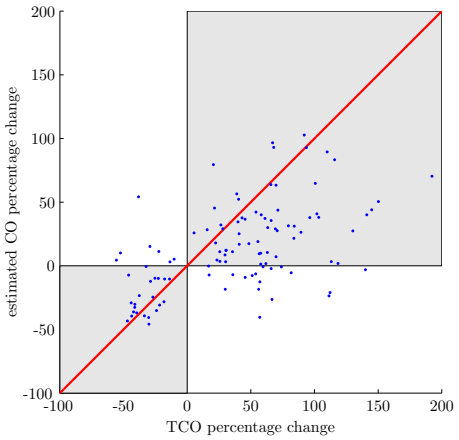

Figure 4-11: Percentage changes in TCO versus estimated CO. Ideally, every point lies on the diagonal line. A point that lies in one of the two shaded zones means that the estimated CO and TCO agree in terms of directional (increase/decrease) change.

Chapter 5

Results and Discussion

5.1 Subject population statistics

First we report the characteristics of the 120 patients studied. Figure 5-1 shows distributions of various population statistics. Table 5.1 lists the the statistical summaries.

Remarks. Although only 78 out of 120 had age data, our study population is mainly composed of the elderly, with no patient under age 40. There are over 1400 TCO measurements with an average value of 5 L/min, which is "textbook normal". Patients typically have a TCO range of 2.5 L/min, which is significantly larger than previous studies of CO estimation performance using human subjects. On average, each patient has 12 TCO measurements over 2.3 days, which is 1 TCO measurement per 4.6 hours. The scarcity in TCO measurements shows the need for CO estimates to fill in the gaps. Mean arterial pressure (P_m) is slightly hypotensive at 75mmHg.

Table 5.1: Population statistics

statistic	mean	SD	units	n
age	69	12	years	78
stay duration	2.3	2.2	days	120
TCO quantity	12	9	N/A	120
ΔTCO per patient	2.5	1.2	L/min	120
ΔP_m per patient	26	11	mmHg	120
ΔPVR per patient	0.5	0.3	mmHg·s/ml	120
cSAI	0.2	0.3	N/A	1436
TCO	5	2	L/min	1436
P_m	75	10	mmHg	1351
heart rate	90	20	bpm	1351
PVR	1	0.4	mmHg·s/ml	1351

Peripheral vascular resistance (PVR) is the ratio of TCO and P_m.

5.2 Removal of poor quality waveforms

As explained in Chapters 3 and 4, waveform quality plays a key role in CO estimation performance. Therefore, ABP waveform segments of poor quality should not be included as part of our performance study. Figure 5-1(c) shows the quality distribution of the 1436

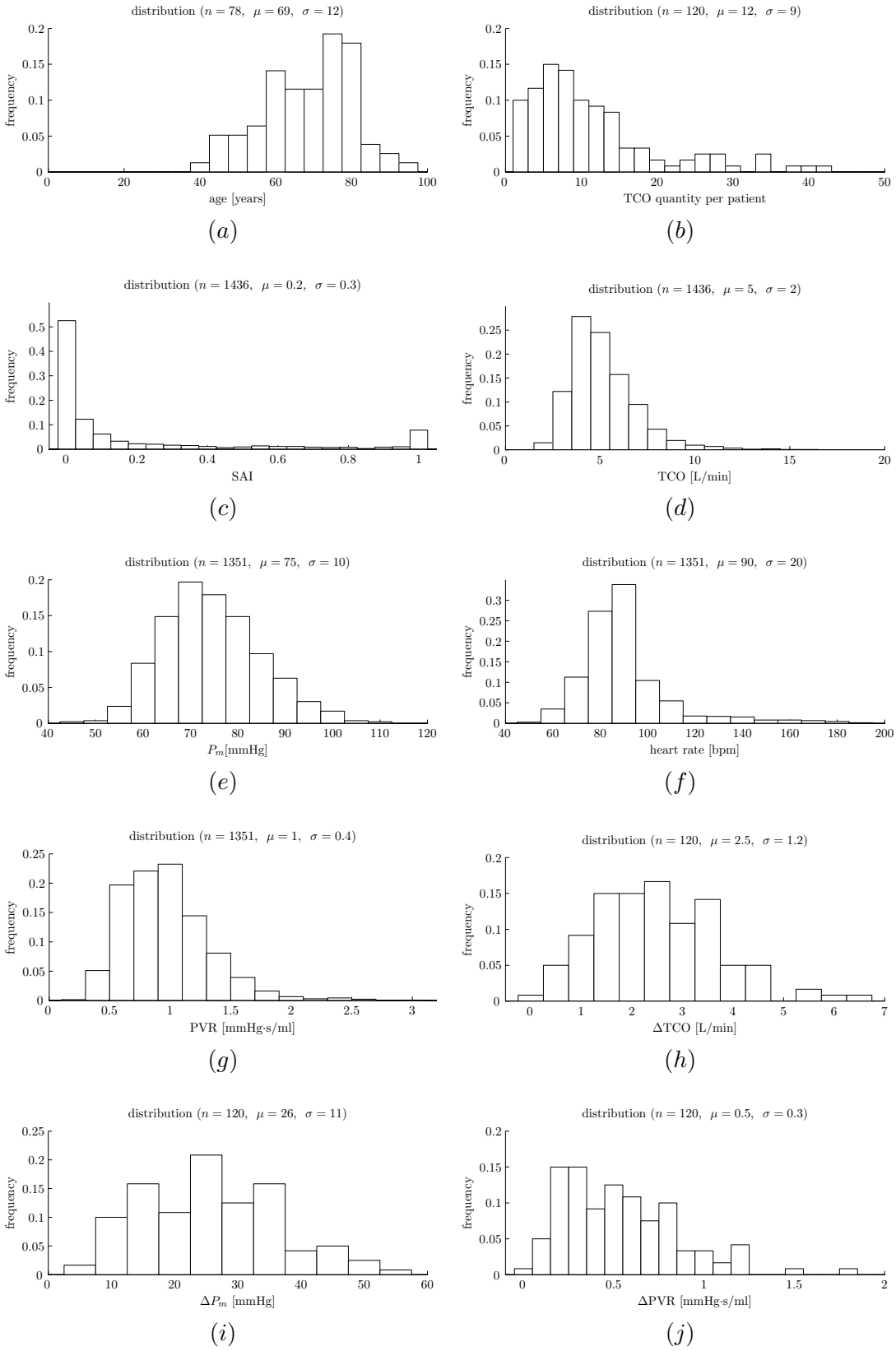

Figure 5-1: Population statistics.

1-min ABP waveforms segments using the cSAI metric. For cSAI, "0" is clean and "1" is completely poor. The majority of waveforms are clean. Based upon this distribution and results shown in Figure 3-7, we decided to only use waveform segments with $cSAI < 0.4$ for our analyses. Figure 5-2 shows the Bland-Altman plot of the Liljestrand algorithm with different levels of signal quality: In (a), all segments are used. In (b), only waveforms with $cSAI < 0.4$ are used. In (c), only the pristine ($cSAI = 0$) waveforms are used. Notice even in (a), the number of comparisons is 1230, not 1436. This is because 120 were used for calibration and the remaining 86 had waveforms of so low quality that features could not be extracted from them. For the rest of this chapter, we only examine CO estimation performance on ABP waveforms with $cSAI < 0.4$.

5.3 Absolute CO estimation

Table 5.2 shows the error of the 11 CO estimators with 3 different calibration methods. C1-calibrated Bland-Altman plots along with error distributions are shown in Figures 5-3 and 5-4. A brief discussion on the statistical significance of the difference between the error distributions can be found in Appendix C. From these results, the best CO estimator is clearly Liljestrand's nonlinear compliance method. Optimal C1 calibration yields a 1 SD error of 0.79 L/min. Most other estimators have errors between 0.9 and 1 L/min. Godje and Wesseling modelflow methods generate particularly large errors. Out of curiosity, we report the error of a hypothetical CO estimator, which maintains constant for each subject. When C1-calibrated, for each subject the constant is close to the mean TCO. When C3-calibrated, that constant is the value of the first TCO data point. The results (last row of Table 5.2 and Figure 5-4f) show that such a constant outperforms all except the Liljestrand method, which indicates that the Liljestrand method is the only method suitable for calibrated CO estimates.

Table 5.2: Estimation error in L/min at 1 SD with 3 different calibration methods. 95% confidence interval errors shown in parentheses. See section 4.3.2 (page 42) for the definition of each calibration method.

Error	C1	C2	C3
Mean arterial pressure	0.97 (2.01)	1.14 (2.33)	1.55 (3.30)
Windkessel	0.98 (1.90)	1.18 (2.32)	1.46 (2.90)
Windkessel RC decay	0.99 (2.00)	1.19 (2.26)	1.46 (2.90)
Herd	1.11 (2.27)	1.33 (2.62)	1.62 (3.40)
Liljestrand nonlinear compliance	0.79 (1.59)	0.95 (1.96)	1.19 (2.43)
Systolic area	0.93 (1.90)	1.10 (2.21)	1.41 (2.95)
Systolic area with correction	0.95 (1.90)	1.13 (2.23)	1.42 (3.05)
Systolic area with corrected impedance	0.91 (1.81)	1.08 (2.14)	1.35 (2.84)
Pressure root-mean-square	0.98 (1.91)	1.19 (2.31)	1.47 (2.95)
Godje nonlinear compliance	1.69 (3.63)	3.25 (5.20)	5.60 (10.94)
Wesseling Modelflow	1.61 (3.37)	1.97 (3.81)	2.80 (6.09)
Constant CO	0.82 (1.66)	0.98 (2.04)	1.36 (2.70)

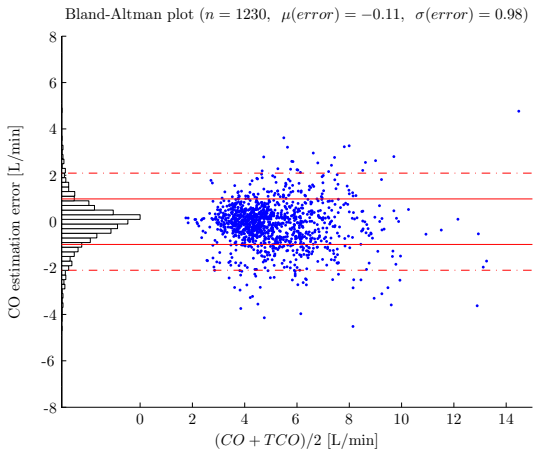

(a) all

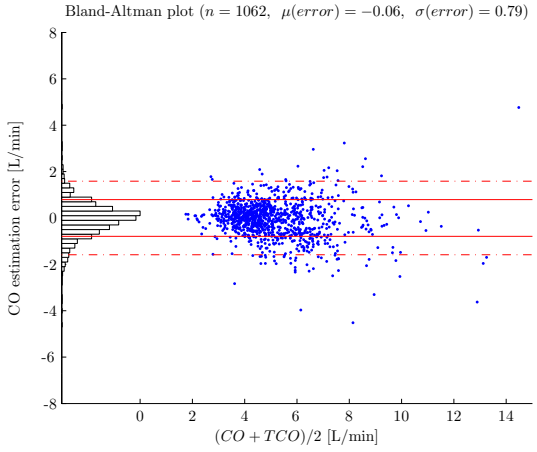

(b) cSAI < 0.4

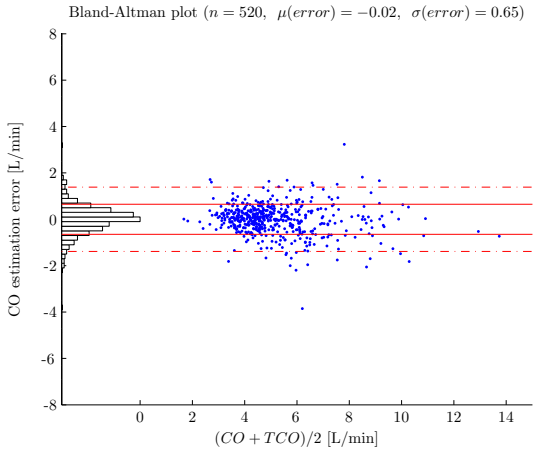

(c) cSAI $= 0$

Figure 5-2: Bland-Altman plots of the Liljestrand CO estimator with various levels of ABP waveform quality: from all inclusive (a) to only the most pristine data (c).

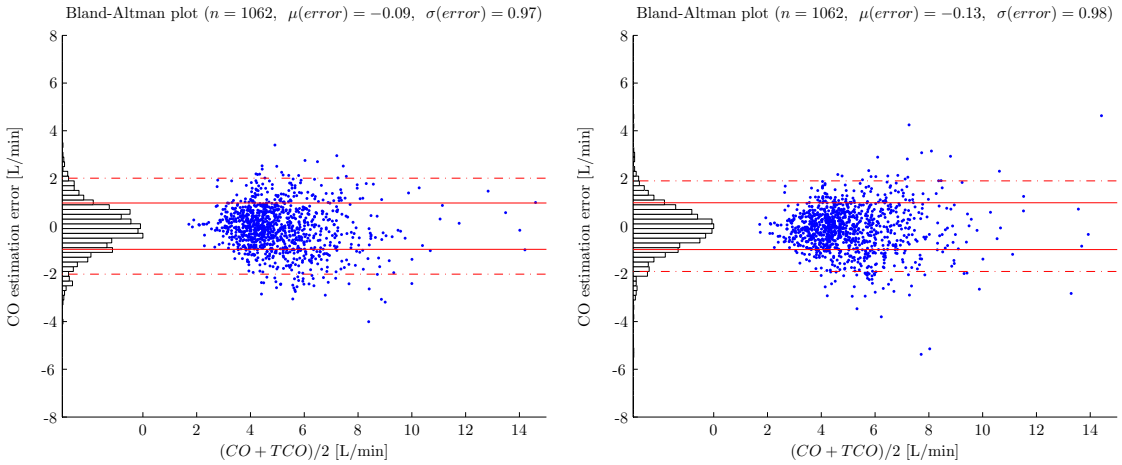

(a) Mean arterial pressure

(b) Windkessel

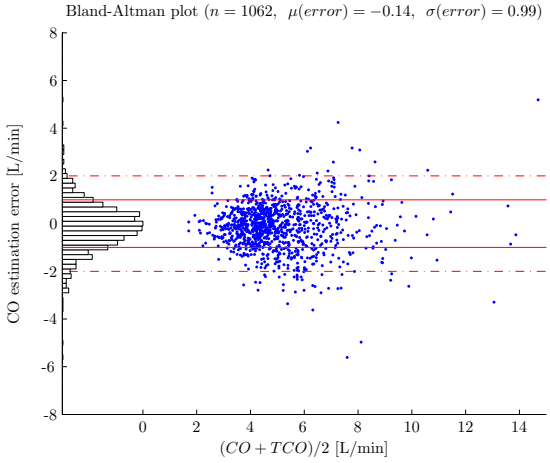

(c) Windkessel RC decay

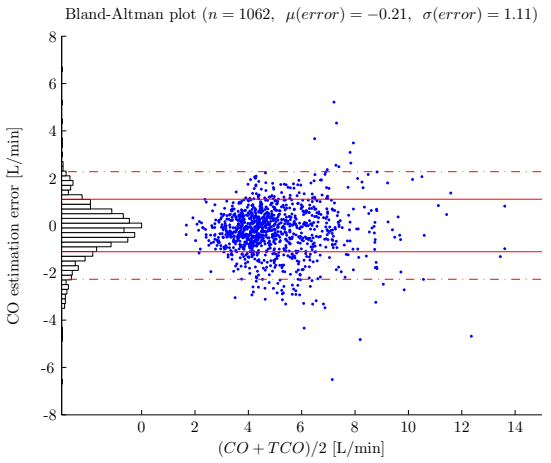

(d) Herd

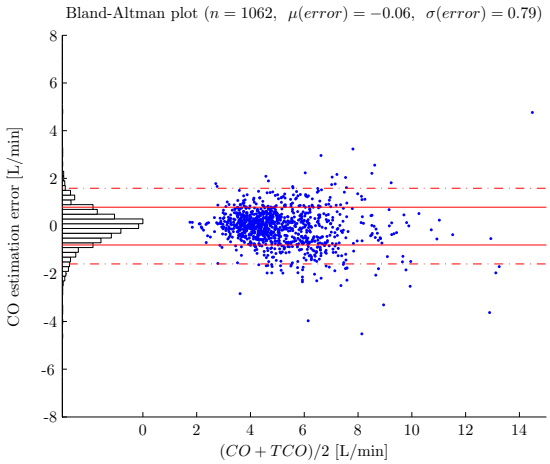

(e) Liljestrand nonlinear compliance

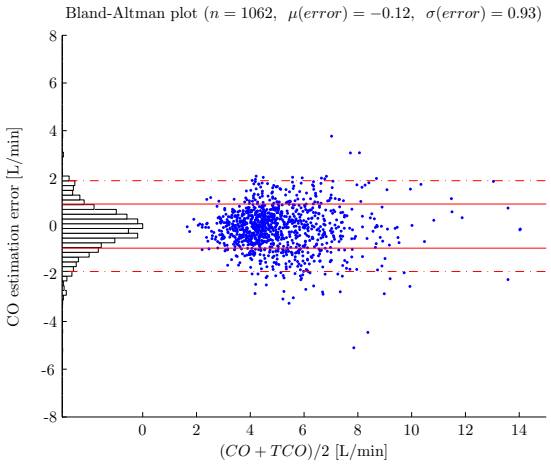

(f) Systolic area

Figure 5-3: Bland-Altman error analysis plots for each CO estimator. The error distribution is shown to the left of each plot. Solid horizontal lines show 1 SD bounds, and dashed lines show 95% confidence intervals.

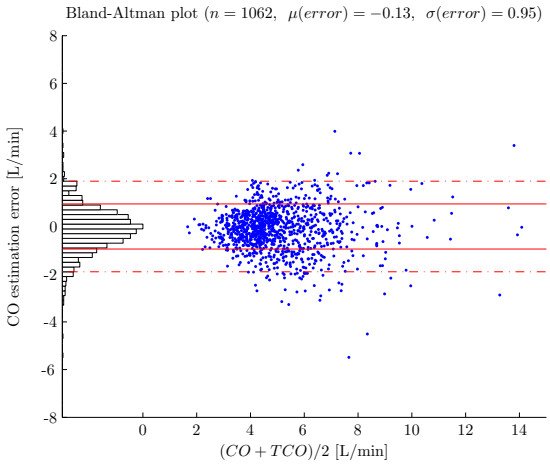

(a) Systolic area with correction

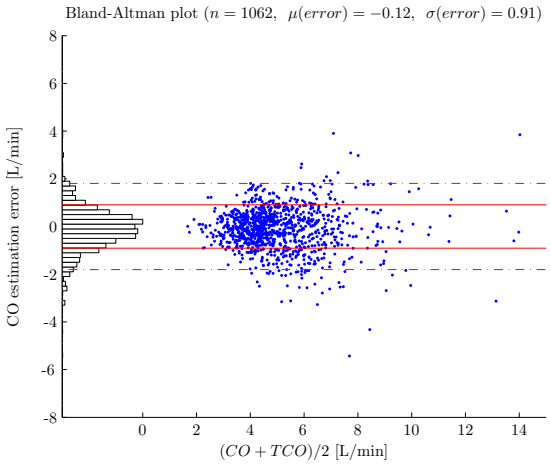

(b) Systolic area with corrected impedance

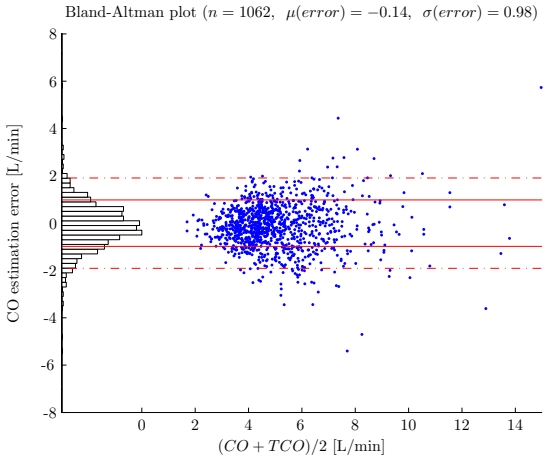

(c) Pressure RMS

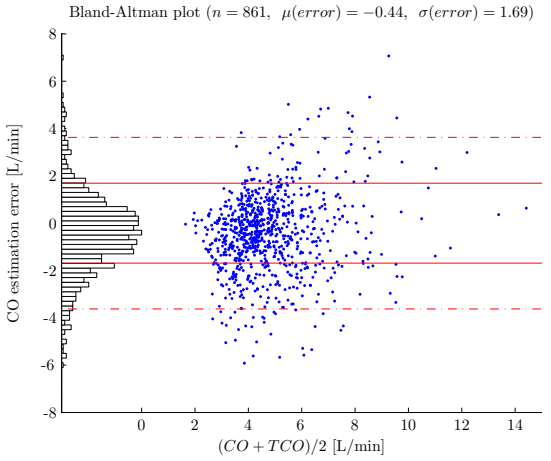

(d) Godje nonlinear compliance

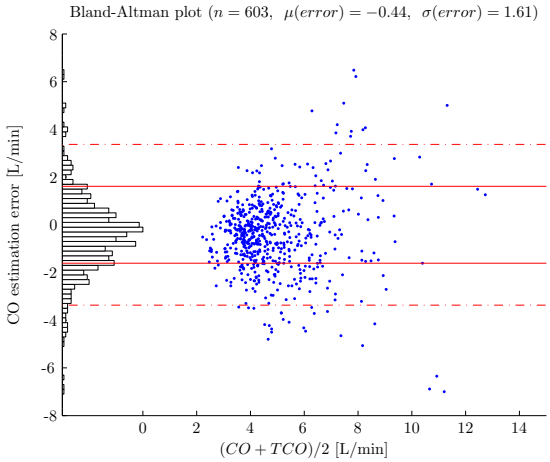

(e) Wesseling Modelflow

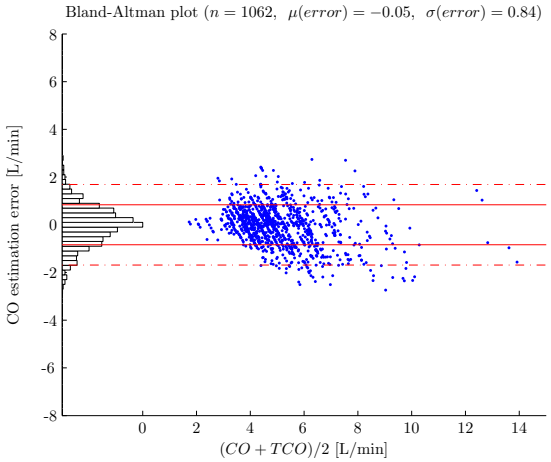

(f) Constant CO

Figure 5-4: Bland-Altman error analysis plots (continued).

5.4 Variability of calibration constants

Table 5.3 shows the variability of C1 and C3 calibration constants across the study population. Liljestrand CO estimator has the lowest C1 and C3 variabilities of 38% and 42%, respectively. These numbers are quite high, indicating that we still must calibrate each patient individually in order to obtain absolute CO estimates.

Table 5.3: Variability of k for C1 and C3 calibration.

Estimator	C1 variability	C3 variability
Mean arterial pressure	0.40	0.50
Windkessel	0.42	0.48
Windkessel RC decay	0.43	0.49
Herd	0.47	0.55
Liljestrand nonlinear compliance	0.38	0.42
Systolic area	0.43	0.48
Systolic area with correction	0.44	0.49
Systolic area with corrected impedance	0.43	0.48
Pressure root-mean-square	0.43	0.48
Godje nonlinear compliance	0.62	1.75
Wesseling Modelflow	0.42	0.51

5.5 Variability of CO estimates

Table 5.4 shows the average variability of beat-to-beat CO estimates obtained from 1-minute ABP waveforms. The P_m CO estimator has the lowest variability of 4%. The more complex estimators have higher variability. These results are plausible because the P_m estimator takes simple averages of all ABP samples whereas the more complex estimators use individual features from the ABP waveform. We do not have the means to prove which CO estimation method has variability levels that closest resembles reality. However, a 10% or less variability in stroke volume does seem reasonable.

Table 5.4: Variability of CO estimates.

Estimator	Variability
Mean arterial pressure	0.04
Windkessel	0.09
Windkessel RC decay	0.10
Herd	0.12
Liljestrand nonlinear compliance	0.07
Systolic area	0.09
Systolic area with correction	0.10
Systolic area with corrected impedance	0.10
Pressure root-mean-square	0.09
Godje nonlinear compliance	0.26
Wesseling Modelflow	0.67

5.6 Relative CO estimation

Figures 5-5 and 5-6 plot percentage changes of estimated CO versus percentage changes in TCO for the 11 CO estimators. Some patients had 50% drops in TCO while others had almost 200% increases. With this large range of TCO increases and decreases, none of the CO estimators are closely clustered around the diagonal line, with the P_m, Godje, and Wesseling modeflow estimators being particularly unsatisfactory. Even the best estimators generate 1 SD errors of 44%. The complete results are reported in Table 5.5. Note that the 1 SD error values should be interpreted with caution due to lack of symmetry: While drops in CO cannot exceed 100%, rises in CO is mathematically unbounded.

However, some estimators work reasonably well in terms of predicting directional (increase/decrease) change. The systolic area with corrected impedance method predicted CO increases correctedly 81% of the time, while the Herd method predicted CO decreses correctedly 83% of the time. Note that the constant CO estimator (Figure 5-6f) doesn't work at all for relative CO estimation. Also, the mean arterial pressure CO estimator has a much smaller dynamic range compared to TCO, as witness by the relatively flat scattergram in Figure 5-5a. This agrees with the cardiovascular physiology theory that the mean pressure is actively controlled (stabilized) to some set point.

Table 5.5: Relative CO estimation error.

Estimator	1SD error	$P(+\|+)$	$P(-\|-)$
Mean arterial pressure	53%	0.49	0.72
Windkessel	48	0.77	0.66
Windkessel RC decay	47	0.78	0.76
Herd	48	0.76	0.83
Liljestrand nonlinear compliance	46	0.80	0.72
Systolic area	46	0.77	0.76
Systolic area with correction	45	0.78	0.76
Systolic area with corrected impedance	44	0.77	0.79
Pressure root-mean-square	46	0.81	0.72
Godje nonlinear compliance	105	0.45	0.62
Wesseling Modelflow	74	0.44	0.69
Constant CO	54	0	0

5.7 Error analysis of selected CO estimators

The Liljestrand method clearly performed the best in absolute CO estimation, had plausible variability levels, and was above average in relative CO estimation. Examining at a finer detail, we now analyze its error as a function of several physiologic parameters. As shown in Figure 5-7, the Liljestrand method becomes more accurate when (a) mean arterial pressure is high, (b) pulse pressure is high, (c) heart rate is low, (d) its own CO estimate is low, (e) systemic resistance is high, and (f) TCO is low. Therefore, when some or all of these conditions are met, we can trust the values given by the Liljestrand algorithm.

The mean arterial pressure method offered similar error characteristics (Figure 5-8 as the Liljestrand method, albeit with larger error magnitudes. The Wesseling Modelflow method has errors of even greater magnitude, as shown in Figure 5-9. Note that the error is especially high if the estimated CO is high (Figure 5-9d).

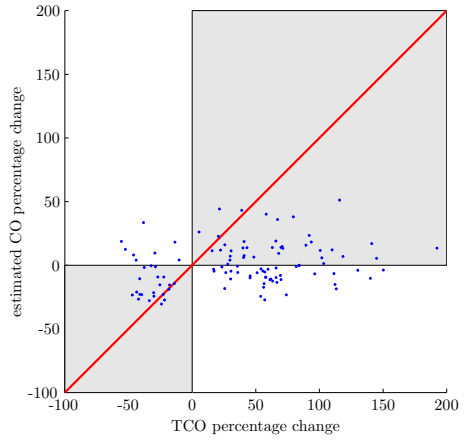

(a) Mean arterial pressure

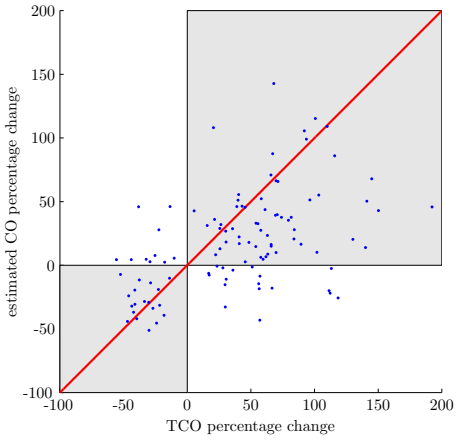

(b) Windkessel

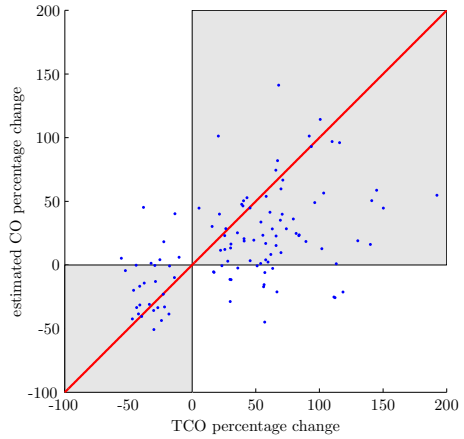

(c) Windkessel RC decay

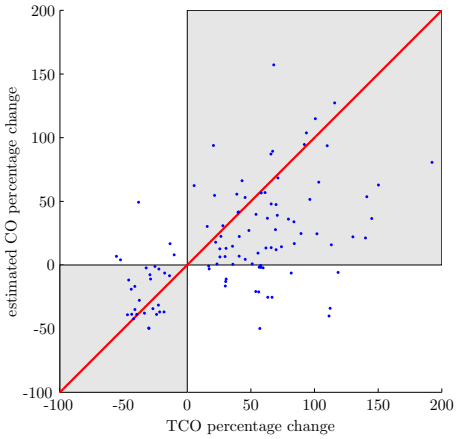

(d) Herd

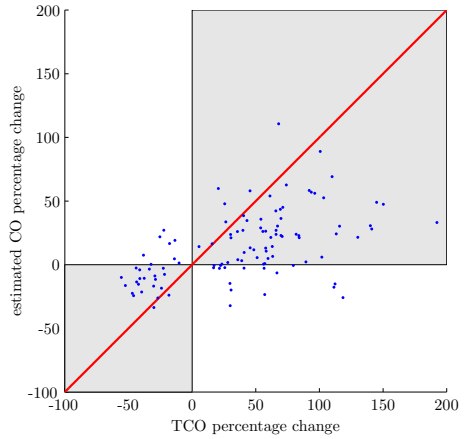

(e) Liljestrand nonlinear compliance

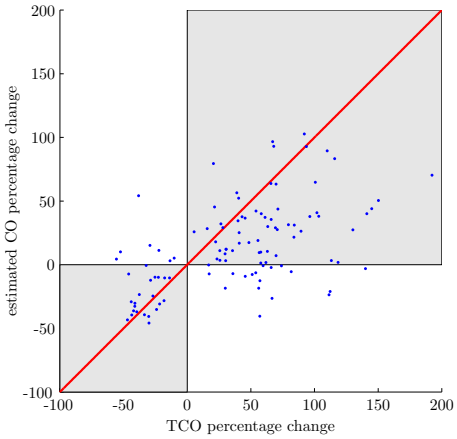

(f) Systolic area

Figure 5-5: Performance of percentages changes in CO. The perfect CO estimator would have data points clustered on the line of identity. Points that fall into the shaded regions signify that the estimator correctedly determined the directional change in CO.

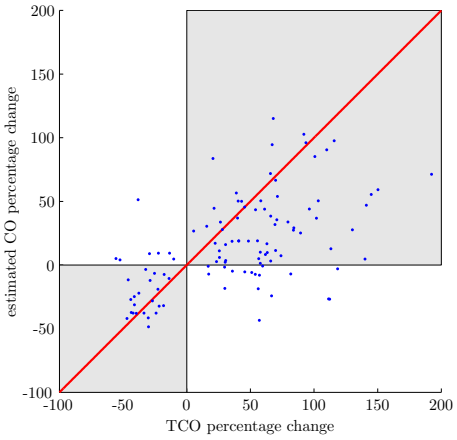

(a) Systolic area with correction

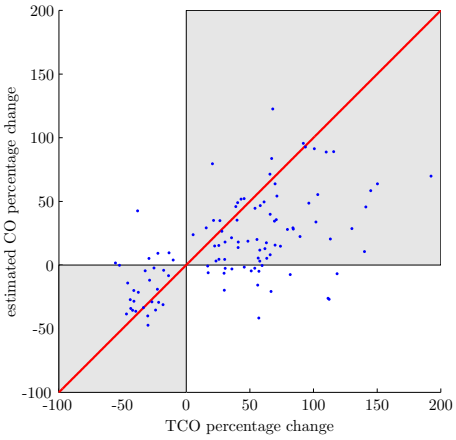

(e) Systolic area with corrected impedance

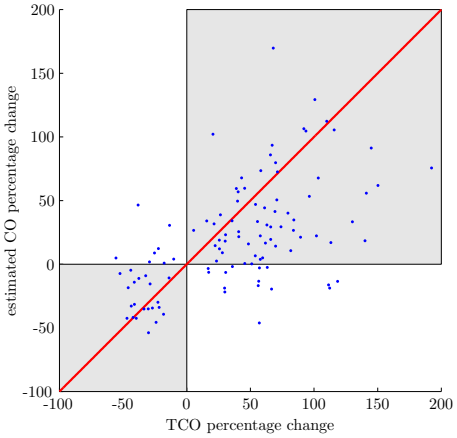

(c) Pressure RMS

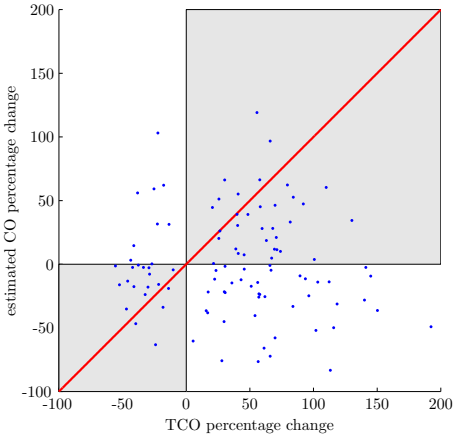

(d) Godje nonlinear compliance

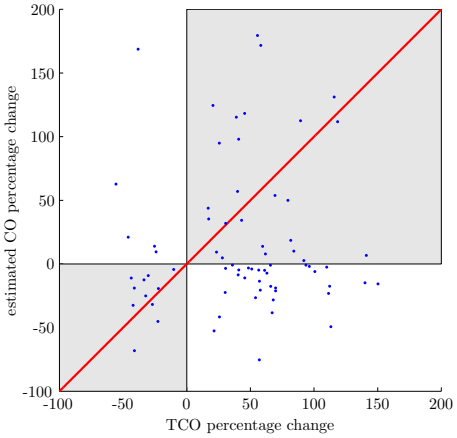

(e) Wesseling Modelflow

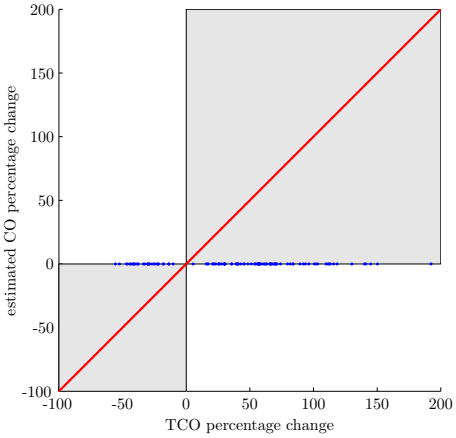

(f) Constant CO

Figure 5-6: Performance of percentages changes in CO (continued).

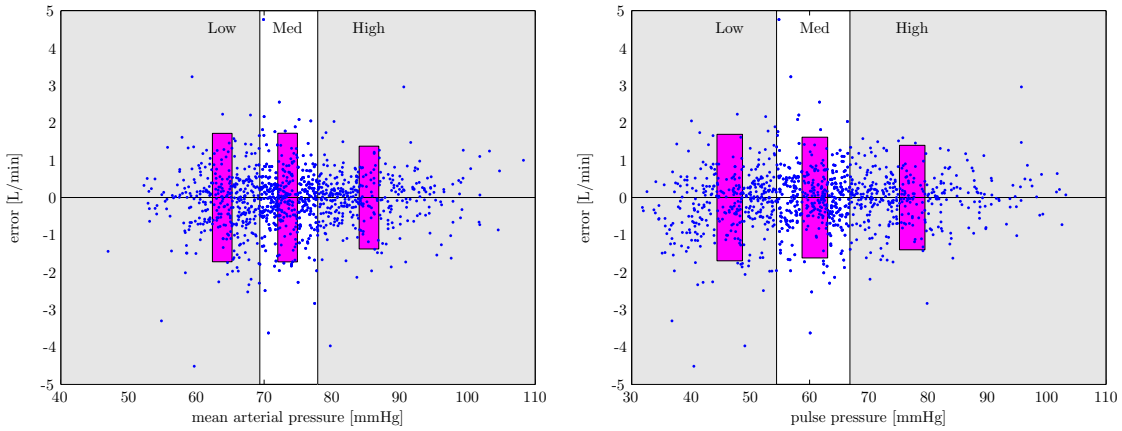

(a)

(b)

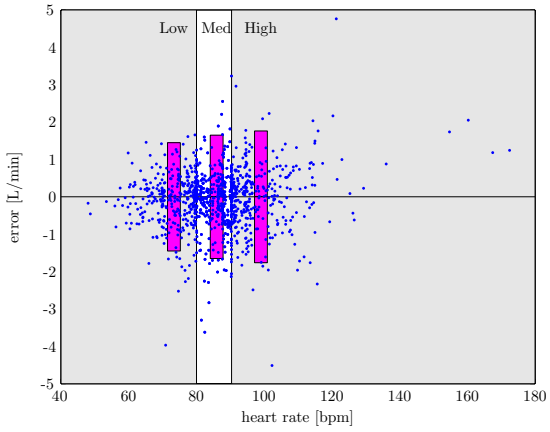

(c)

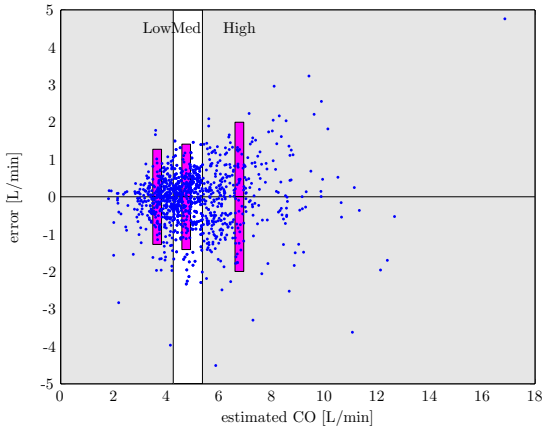

(d)

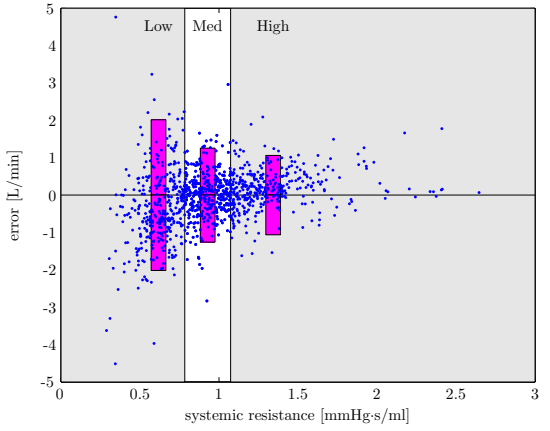

(e)

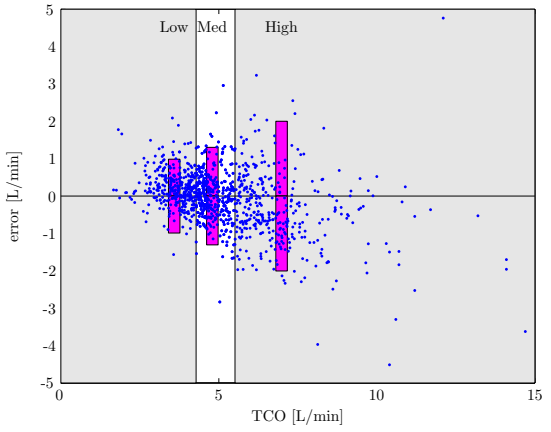

(f)

Figure 5-7: CO estimation (Liljestrand method) error as a function of several variables. Each variable is segmented into low, medium, and high regions with equal quantity. Rectangular bars represent the 95% confidence intervals.

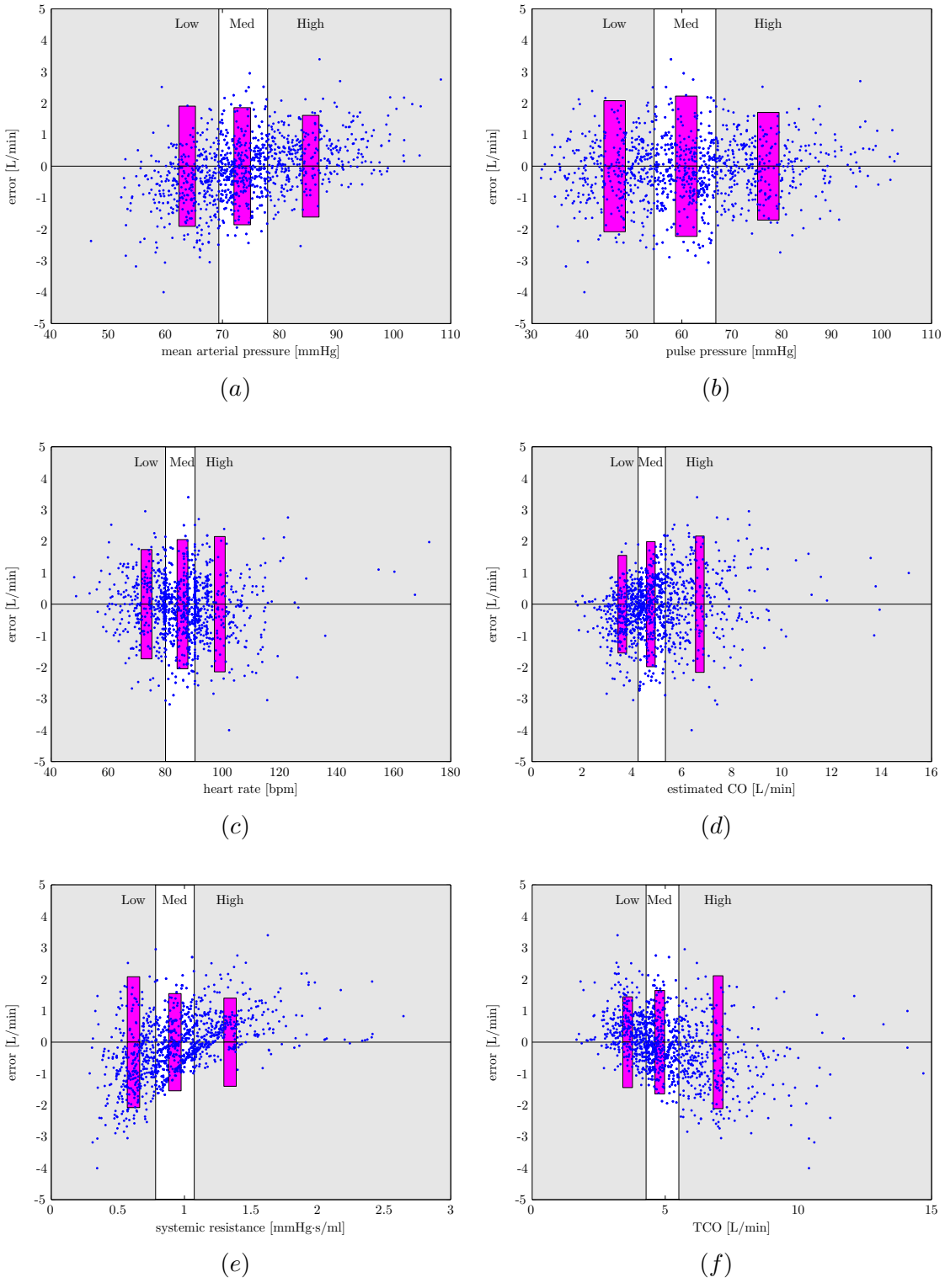

Figure 5-8: CO estimation (mean arterial pressure method) error as functions of several variables.

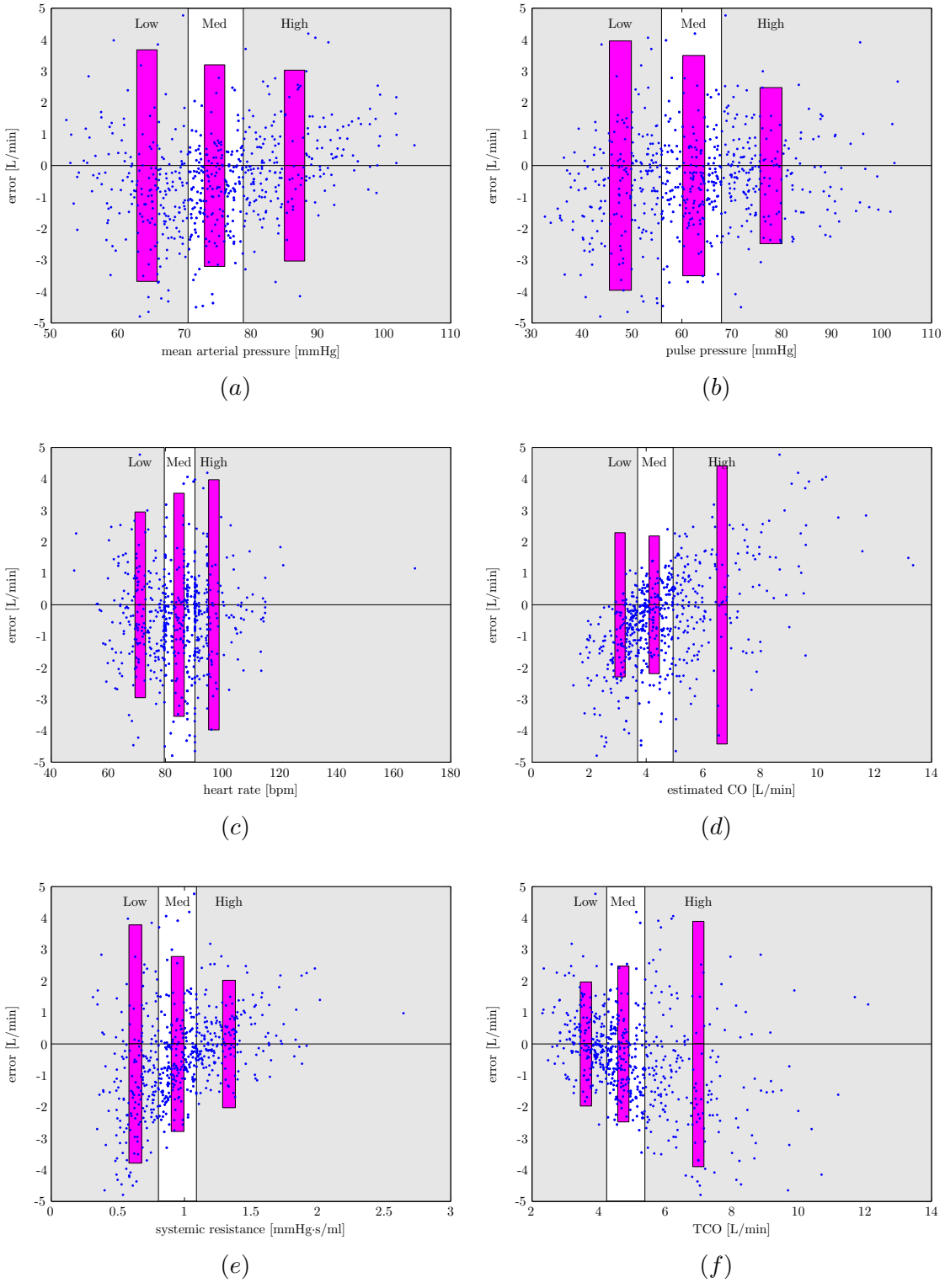

Figure 5-9: CO estimation (Wesseling Modelflow method) error as functions of several variables.

5.8 Selected time series case studies

Up until now, this chapter has focused upon reporting error statistics of each CO estimator. The champion is the Liljestrand method. In this section, we selected two subjects to examine the time series data of Liljestrand CO estimates.

Subject: caseID 8463. This subject has 14 TCO measurements between 3.4 and 5.8 L/min. As shown in Figure 5-10, the error between TCO and Liljestrand estimated CO is small. The large increase and decrease in TCO between minute 1000 and 1700 are captured by corresponding dynamical changes in mean pressure and heart rate.

Subject: caseID 6629. This subject is a 70 year old male with aortic valve disease. His 5 TCO measurements are between 5.2 and 7.3 L/min. His left ventricular ejection fraction is 41%, which is lower than the normal range of 55-75%. As shown in Figure 5-11, the error between TCO and Liljestrand CO estimates is more prominent here: TCO increased significantly from the 3rd to 4th TCO measurement while pulse pressure, mean pressure, and heart rate remained relatively constant in this time frame, which collectively yields a constant Liljestrand CO estimate.

5.9 Discussion

One burdening question: Are CO values, when estimated from the ABP waveform, accurate enough for clinical use? The answer is not so simple. First, we must revisit the accuracy of thermodilution CO (TCO). According to Stetz et al. [17], TCO has a 1SD error of about 10%, which is 0.5 L/min when assuming a nominal CO of 5 L/min. Comparatively, the Liljestrand estimator generated errors of 0.8 L/min when optimally calibrated and 1.2 L/min when scantily calibrated. Thus, the best CO estimation method has an error that is approximately twice that of TCO. Now, is twice the error still accurate enough for clinical use? Clinicians typically care most about substantial changes in CO. For each patient in our study population, the average TCO range was 2.5 L/min (Table 5.1). For a change in CO of 2.5 L/min, the Liljestrand method should certainly be able to distinguish such an event.

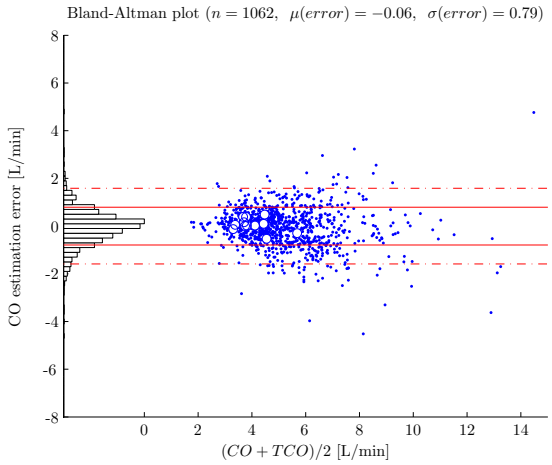

(a)

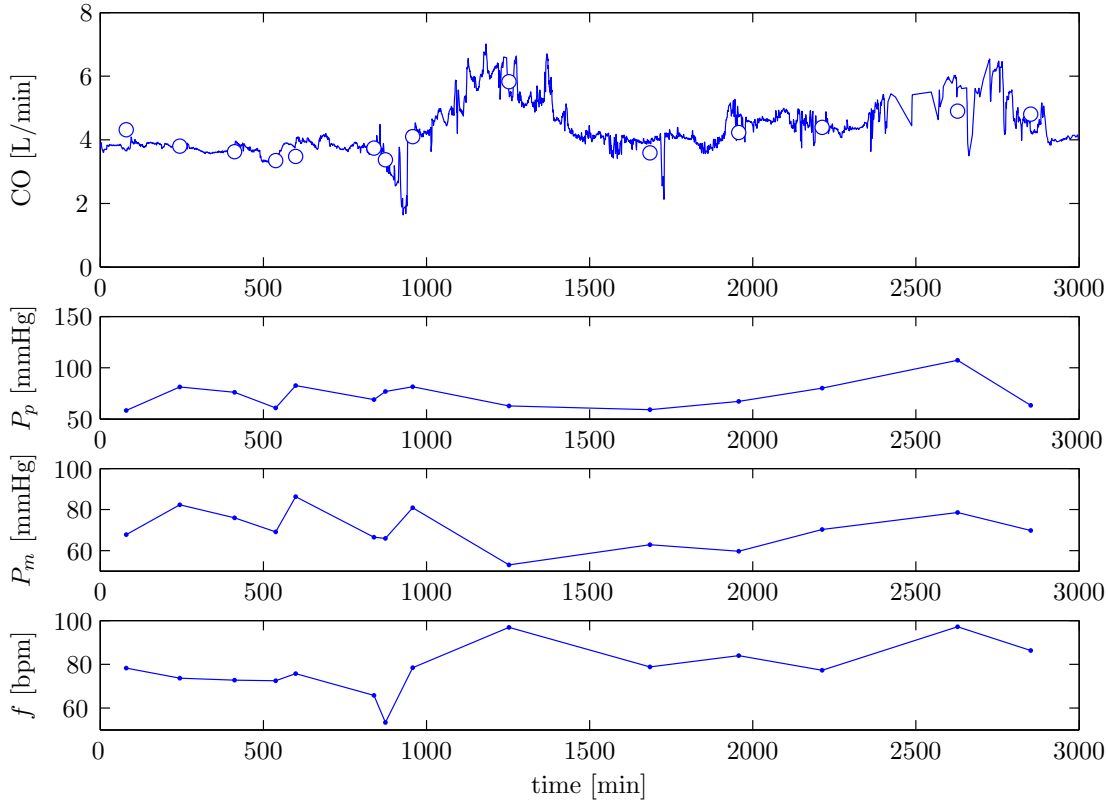

(b)

Figure 5-10: Time series of caseID 8463 using the Liljestrand CO estimator. (a) Bland-Altman plot with estimation error from caseID 8463 highlighted. (b) Top plot shows continuous Liljestrand CO estimates with TCO data points superimposed. Bottom 3 plots shows the components of the Liljestrand CO estimator: pulse pressure, mean pressure, and heart rate.

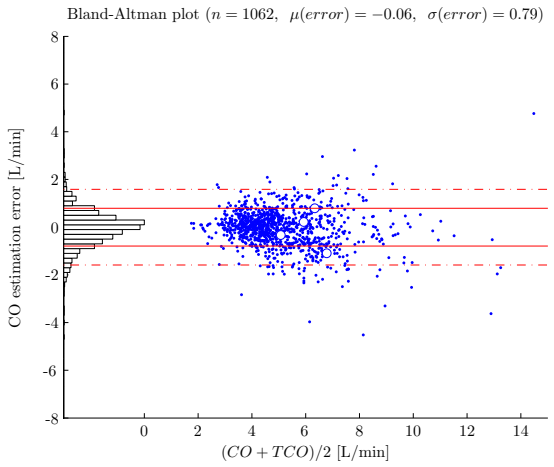

(a)

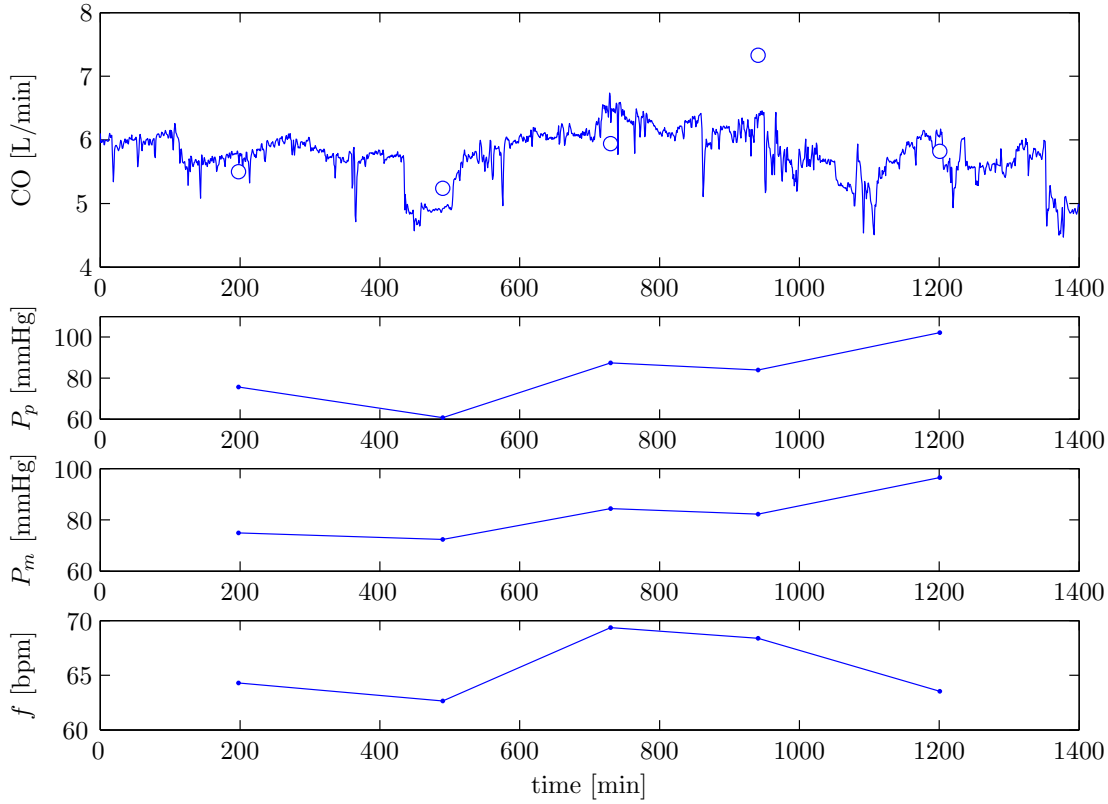

(b)

Figure 5-11: Time series of caseID 6629 using the Liljestrand CO estimator. Compared to the previous subject, CO estimation performance is worse here. TCO increased significantly from the 3rd to 4th data point, but pulse pressure, mean pressure, and heart rate remained relatively constant.

Chapter 6

Conclusions and Future Research

6.1 Summary

In this thesis we have presented and evaluated 11 of the established cardiac output estimation methods using ABP waveform data from the MIMIC II database.

Chapter 2 discussed the theoretical basis of each CO estimation method. The simplest method was based upon a drastically simplified model of the cardiovascular system. The most complex method, Wesseling's modelflow, was based upon a model with many nonlinearities in an attempt to more accurately characterize the dynamics of the cardiovascular system. Chapter 2 concluded with a discussion on the fundamental limitations of estimating CO using ABP waveforms.

Chapter 3 addressed one limitation that hindered CO estimation performance: ABP waveform quality. The signal abnormality index (SAI) algorithm presented in this chapter attempted to flag regions of ABP waveform of poor quality. In defining what constitutes a poor ABP waveform, we tried to be as objective as as possible. Output of the algorithm was mostly in concordance with a human expert and proven to be effective in reducing CO estimation error.

Chapter 4 presented our methods for evaluating the CO estimators. We designed algorithms to extract pressure and temporal features from the ABP waveform. We integrated the SAI algorithm to ensure that extremely poor ABP waveforms are eliminated. We designed calibration techniques, which is necessary for CO estimators to produce absolute values in liters per minute. In absence of calibration, we presented a technique to compare percentage changes in gold-standard CO with percentage changes in estimated CO.

Chapter 5 showed the performance of the 11 CO estimators. For absolute CO estimation, the Liljestrand CO estimator was clearly the champion. It generated errors of 0.8 L/min when optimally calibrated and 1.2 L/min when scantily calibrated. Whether such specifications are meritable for clinical use is ultimately up to the decision of a clinician. However, it should be noted that patients with life-threatening problems often have CO fluctuations significantly beyond 1.2 L/min. For each patient in our study population, the average thermodilution CO range was 2.5 L/min. Thus, the Liljestrand estimator should be able to detect such large changes in CO.

6.2 Suggestions for future research

As this thesis draws to a close, inevitably there are research tasks not accomplished but would be plausible extensions of this thesis. There are also interesting research tangents to embark on.

Algorithmic improvements. As evidenced by the 11 CO estimators studied in this thesis, previous research on improving CO estimation have been mostly in the creation of new methods from first principles or in the modification of existing methods. An alternative approach to improve CO estimation is to optimally combine the existing methods. It is likely that one CO algorithm works better than another under different physiologic situations. The detailed error analysis of the Liljestrand algorithm (Figure 5-7) clearly shows that this algorithm is more accurate when mean arterial pressure is over 80mmHg, heart rate is less than 80bpm, estimated CO is less than 5L/min, and systemic resistance is greater than 1 mmHg·s/ml. We can perform similar error analysis on the remaining 10 algorithms, perhaps as a function of even more physiologic information obtained from lab tests and nursing notes. Then, a master algorithm may be developed to optimally choose the CO estimator(s) that will likely be most accurate for each particular patient.

The Signal Abnormality Index (SAI) algorithm works reasonably well but certainly has potential for improvement. The current SAI logic is composed of a series of static criteria imposed on pressure values and beat-to-beat durations (Table 3.2). Each criterion is independent of each other. One possible improvement would be to dynamically change the thresholds for each criterion. For example, beat-to-beat variations of systolic blood pressure is likely larger in patients with large pulse pressure than ones with small pulse pressure. Thus, abnormality criteria 7 in Table 3.2 should be a function of pulse pressure rather than the constant value of 20mmHg. However, with rising complexity, the degrees of freedom in the algorithm rises, and one must attempt to avoid over-training the algorithm to a particular data set.

Live clinical evaluations. All research in this thesis have been in analyzing data retrospectively. It does not prove that continuous cardiac output monitoring with such a level of accuracy can indeed aid in clinical decision making. It would be an interesting investigation to build a CO bedside monitoring system (perhaps in addition to providing CO estimates, the system would generate alarms when CO exceeds a nominal range or undergoes dramatic change) and use it in a hospital to see whether such a system provides clinicians with valuable information that is not available otherwise.

Stroke volume variability. Variabilities of CO estimates are different amongst the estimation methods. By removing heart rate out of the equation, we can obtain variability of stroke volume, which raises a couple of interesting questions. First, which method of obtaining stroke volume gives the variability level that closest resembles reality? Second, does an increase in stroke volume variability of a patient forewarn the onset of certain disease processes? Is stroke volume variability closely coupled with heart rate variability? Querying for "heart rate variability" yields 5644 articles on PubMed online. Querying "stroke volume variability" yields a scant 6 articles, which means there may be new research potential here.

Appendix A

Notation Summary

Table A.1: Commonly used acronyms and symbols

symbol	**description**	**units**
Q, CO	cardiac output	L/min
$q(t)$	instantaneous pulsatile flow	ml/s
$P(t)$, ABP	arterial blood pressure	mmHg
P_m	mean arterial pressure	mmHg
P_s	systolic pressure	mmHg
P_d	diastolic pressure	mmHg
P_p	pulse pressure ($P_s - P_d$)	mmHg
f	heart rate	beats per minute
T	beat duration ($60/f$)	sec
T_s	duration of systole	sec
T_d	duration of diastole ($T - T_s$)	sec
R, SVR, PVR	systemic resistance	mmHg·s/ml
C	arterial capacitance (compliance)	ml/mmHg
A_s	area under $P(t)$ during systole	mmHg·s

Appendix B

Selected Code Descriptions

All MATLAB code may be obtained at http://mimic.mit.edu/svn/jco/trunk/, provided that you have access permissions.

B.1 wavex.m

```
WAVEX Arterial blood pressure waveform extractor.
  WAVEX(CASEID,INDIR,OUTF) extracts entire ABP waveform of CASEID in the
  directory INDIR, then store as MAT-file named OUTF.

  In:   CASEID (integer)  e.g. caseid=3784;
        INDIR  (string)   e.g. indir='01-11-08/m2w03784/';
        OUTF   (string)   e.g. outf='/tmp/p3784';

  Out:  OUTF.mat  Within this MAT-file, there are variables:
        abp* --- continuous abp waveform segments
        t0   --- col 1: initial time of each ABP segment
                     2: # of samples of each ABP segment
        source_file --- cell array containing WFDB file name of ABP segs

  Usage:
  - Make sure wfdb package is installed for linux
  - wfdb_tools for MATLAB is required
```

B.2 trendex.m

```
TRENDEX MIMIC II trend extractor
  Y = TRENDEX(CASEID,FNAME,TREND) extracts TREND of CASEID from file FNAME.

  In:   caseid (integer)  e.g. caseid=3784;
        fname  (string)   e.g. fname='trends/01-11-08/004_m2t03784';
        trend             e.g. trend='CO' or trend='HR' or trend='all';

  Out:  <1x1> struct
         Y.caseid --- caseid
         Y.t0     --- absolute starting time of record (datenum format)
         Y.CO     --- <kx2> matrix containing time offset (minutes) from
                      beginning of record and corresponding CO (L/min)
         Y...     --- examine the struct for more possible trends
```

```
  Usage:
  - Make sure wfdb package is installed for linux
  - wfdb_tools for MATLAB is required
  - if 3rd argument is 'all', then all trends of CASEID are obtained
```

B.3 wabp.m

```
WABP  ABP waveform onset detector.
  r = WABP(ABP) obtains the onset time (in samples)
      of each beat in the ABP waveform.

  In:   ABP (125Hz sampled)
  Out:  Onset sample time

  Usage:
  - ABP waveform must have units of mmHg
```

B.4 abpfeature.m

```
ABPFEATURE  ABP waveform feature extractor.
  r = ABPFEATURE(ABP,ONSETTIMES) extracts features from ABP waveform such
  as systolic pressure, mean pressure, etc.

  In:   ABP (125Hz sampled), times of onset (in samples)
  Out:  Beat-to-beat ABP features
          Col 1:  Time of systole   [samples]
              2:  Systolic BP       [mmHg]
              3:  Time of diastole  [samples]
              4:  Diastolic BP      [mmHg]
              5:  Pulse pressure    [mmHg]
              6:  Mean pressure     [mmHg]
              7:  Beat Period       [samples]
              8:  mean_dyneg
              9:  End of systole time  0.3*sqrt(RR)  method
             10:  Area under systole   0.3*sqrt(RR)  method
             11:  End of systole time  1st min-slope method
             12:  Area under systole   1st min-slope method

  Usage:
  - OnsetTimes must be obtained using wabp.m
```

B.5 jSQI.m

```
JSQI  ABP waveform signal quality index.
  [BEATQ, R] = JSQI(FEATURES, ONSET, ABP) returns a binary signal quality
  assessment of each beat in ABP.  This algorithm relies on detecting
  abnormalities of numeric values in FEATURES and ONSET.

  In:   FEATURES <mx12> --- features extracted from ABP using abpfeature.m
        ONSET    <nx1>  --- onset times of ABP using wabp.m
        ABP      <px1>  --- arterial blood pressure waveform (125Hz sampled)
```

```
Out:  BEATQ    <nx10> --- SQI of each beat: 0=good, 1=bad
        Col 1:  logical OR of cols 2 thru 10
            2:  P   not physiologic  (<20 or >300 mmHg)
            3:  MAP not physiologic  (<30 or >200 mmHg)
            4:  HR  not physiologic  (<20 or >200 bpm)
            5:  PP  not physiologic  (<30 mmHg)
            6:  abnormal Psys        (beat-to-beat change > 20 mmHg)
            7:  abnormal Pdias       (beat-to-beat change > 20 mmHg)
            8:  abnormal period      (beat-to-beat change > 1/2 sec)
            9:  abnormal P(onset)    (beat-to-beat change > 20 mmHg)
           10:  noisy beat           (mean of negative dP < -3)
      R        <1x1>  fraction of good beats in ABP

  Usage:
  - FEATURES must be obtained using abpfeature.m
  - ONSET    must be obtained using wabp.m
```

B.6 estimateCO.m

```
 ESTIMATECO  Cardiac output estimator.
   [CO, TO, TOLD, FEA] = ESTIMATECO(FNAME, ESTID, FILT_ORDER) is the
   main function for estimating cardiac output.

   In:   FNAME      <1xn>  --- file where ABP and features are located
         ESTID      <1x1>  --- the CO estimator to use
         FILT_ORDER <1x1>  --- order of running avg LPF to use on output
                                  (enter 0 or 1 for no LPF)

   Out:  CO         <kx1>  --- estimated CO (uncalibrated)
         TO         <kx1>  --- time [minutes] (not evenly sampled!)
         TOLD       <mx1>  --- time [minutes], not sqi filtered
         FEA        <kx11> --- feature matrix

   Usage:
   This function is only a wrapper.  Actual CO estimation computation is
   done in the following required functions:
   ESTID 1: est01_MAP      - Mean pressure
         2: est02_WK       - Windkessel 1st order LTI RC circuit model
         3: est03_SA       - Systolic area distributed model
         4: est04_SAwarner - Warner systolic area with time correction
         5: est05_Lilj     - Liljestrand PP/(Psys+Pdias) estimator
         6: est06_Herd     - Herd estimator
         7: est07_SAwessCI - Wesseling systolic area with impedance correction
         8: est08_Pulsion  - Pulsion non-linear compliance model
         9: est09_LidCO    - LidCO root-mean-square model
        10: est10_RCdecay  - RC exponential decay fit
        11: est11_mf       - Wesseling non-linear, time-varying 3-element model
```

Appendix C

Test of Statistical Significance

Table C.1 below shows the p-values using the Kolmogorov-Smirnov test (KS test). The KS test performs pairwise comparisons of error distributions (Figures 5-3, 5-4) between the CO estimation methods. Table C.2 corresponds the method numbers in Table C.1 with the actual names.

Table C.1: p-values using the Kolmogorov-Smirnov test.

Method	2	3	4	5	6	7	8	9	10	11	12
1	0.68	0.29	0.07	1.2e-4	0.27	0.20	0.05	0.50	4.7e-15	9.8e-12	6.1e-3
2		1	0.22	1.8e-4	0.43	0.96	0.37	0.95	8.8e-15	2.6e-11	1.1e-3
3			0.32	5.5e-5	0.46	0.90	0.22	0.98	1.9e-14	4.8e-11	6.3e-4
4				7.6e-8	0.02	0.04	4.5e-3	0.29	4.7e-11	4.4e-8	1.3e-7
5					6.1e-3	1.3e-3	8.2e-3	8.2e-5	3.0e-29	2.2e-23	0.02
6						0.88	0.99	0.32	8.4e-17	3.5e-14	0.01
7							0.64	0.85	3.1e-16	1.0e-12	3.7e-4
8								0.32	9.9e-19	1.1e-14	8.2e-3
9									6.4e-14	8.0e-11	2.0e-5
10										0.55	1.4e-24
11											2.9e-19

Table C.2: Labels for CO estimation methods.

CO estimation method	Label
Mean arterial pressure	1
Windkessel	2
Windkessel RC decay	3
Herd	4
Liljestrand nonlinear compliance	5
Systolic area	6
Systolic area with correction	7
Systolic area with corrected impedance	8
Pressure root-mean-square	9
Godje nonlinear compliance	10
Wesseling Modelflow	11
Constant CO	12

Bibliography

[1] HC Bazett. An analysis of the time-relations of electrocardiograms. *Heart*, 7:353–370, 1920.

[2] RM Berne, MN Levy, BM Koeppen, and BA Stanton. *Physiology*. Mosby, 5th edition, 2004.

[3] JM Bland and DG Altman. Statistical methods for assessing agreement between two methods of clinical measurement. *The Lancet*, pages 307–310, 1986.

[4] J Bourgeois, B Gilbert, D Donald, and E Wood. Characteristics of aortic diastolic pressure decay with application to continuous monitoring of changes in peripheral vascular resistance. *Circulation Research*, 35:56–66, 1974.

[5] J Erlanger and BR Hooker. An experimental study of blood pressure and pulse-pressure in man. *Johns Hopkins Hospital Report*, 12:145–378, 1904.

[6] O Godje, P Lamm, C Schmitz, M Theil, and B Reichart. Continuous, less invasive, hemodynamic monitoring in intensive care after cardiac surgery. *Thoracic Cardiovascular Surgery*, 46:242–249, 1998.

[7] JA Herd, NR Leclair, and W Simon. Arterial pressure pulse contours during hemorrhage in anesthetized dogs. *Journal of Applied Physiology*, 21(6):1864–1868, 1966.

[8] LL Huntsman, DK Stewart, SR Barnes, SB Franklin, JS Colocousis, and EA Hessel. Noninvasive doppler determination of cardiac output in man: clinical validation. *Circulation*, 67:593–602, 1983.

[9] M Jonas, D Hett, and J Morgan. Real time, continuous monitoring of cardiac output and oxygen delivery. *International Journal of Intensive Care*, 9(2), 2002.

[10] NT Kouchoukos, LC Sheppard, and DA McDonald. Estimation of stroke volume in the dog by a pulse contour method. *Circulation Research*, 26:611–623, 1970.

[11] GJ Langewouters, KH Wesseling, and WJA Goedhard. The static elastic properties of 45 human thoracic and 20 abdominal aortas in vitro and the parameters of a new model. *Journal of Biomechanics*, 17:425–435, 1984.

[12] G Liljestrand and E Zander. Vergleichende bestimmungen des minutenvolumens des herzens beim menschen mittels der stickoxydulmethode und durch blutdruckmessung. *Z Ges Exp Med*, 59:105–122, 1928.

[13] RG Mark. MIT course notes for 6.022J quantitative physiology — cardiovascular mechanics. http://mit.edu/6.022j/www/, 2005.

[14] R Mukkamala, AT Reisner, RG Mark, and RJ Cohen. Continuous cardiac output monitoring by peripheral blood pressure waveform analysis. *IEEE Transactions on Biomedical Engineering*, 53:459–467, 2006.

[15] WW Nichols and MF O'Rourke. *McDonald's Blood Flow in Arteries.* Arnold, 4th edition, 1998.

[16] M Saeed, C Lieu, G Raber, and RG Mark. MIMIC II: A massive temporal ICU patient database to support research in intelligent patient monitoring. In *Computers in Cardiology*, volume 29, pages 641–644, 2002.

[17] CW Stetz, RG Miller, GE Kelly, and TA Raffin. Reliability of the thermodilution method in the determination of cardiac output in clinical practice. *American Review of Respiratory Disease*, 126(6):1001–4, 1982.

[18] JJ van Lieshout and KH Wesseling. Editorial II: Continuous cardiac output by pulse contour analysis? *British Journal of Anaesthesia*, 86(4):467–468, 2001.

[19] HR Warner, HJC Swan, DC Connolly, RG Tompkins, and EH Wood. Quantitation of beat-to-beat changes in stroke volume from the aortic pulse contour in man. *Journal of Applied Physiology*, 5:495–507, 1953.

[20] KH Wesseling, R Jansen, J Settels, and J Schreuder. Computation of aortic flow from pressure in humans using a nonlinear, three-element model. *Journal of Applied Physiology*, 74(5):2566–2573, 1993.

[21] KH Wesseling, BD Wit, JAP Weber, and NT Smith. A simple device for the continuous measurement of cardiac output. *Advanced Cardiovascular Physiology*, 5(2):16–52, 1983.

[22] W Zong, T Heldt, GB Moody, and RG Mark. An open-source algorithm to detect onset of arterial blood pressure pulses. In *Computers in Cardiology*, volume 30, pages 259–262, 2003.